Review

Designing Smart Iron Oxide Nanoparticles for MR Imaging of Tumors

Zhenzhen Li, Ru Bai, Jia Yi, Huige Zhou,* Junfang Xian,* and Chunying Chen*

Cite This: *Chem. Biomed. Imaging* 2023, 1, 315–339

Read Online

ACCESS | Metrics & More | Article Recommendations

ABSTRACT: Iron oxide nanoparticles (IONPs) possess unique magnetism and good biocompatibility, and they have been widely applied as contrast agents (CAs) for magnetic resonance imaging (MRI). Traditional CAs typically show a fixed enhanced signal, thus exhibiting the limitations of low sensitivity and a lack of specificity. Nowadays, the progress of stimulus-responsive IONPs allows alteration of the relaxation signal in response to internal stimuli of the tumor, or external stimuli, thus providing an opportunity to overcome those limitations. This review summarizes the current status of smart IONPs as tumor imaging MRI CAs that exhibit responsiveness to endogenous stimuli, such as pH, hypoxia, glutathione, and enzymes, or exogenous stimuli, such as magnets, light, and so on. We discuss the challenges and future opportunities for IONPs as MRI CAs and comprehensively illustrate the applications of these stimuli-responsive IONPs. This review will help provide guidance for designing IONPs as MRI CAs and further promote the reasonable design of magnetic nanoparticles and achieve early and accurate tumor detection.

KEYWORDS: *Iron oxide nanoparticles, Magnetic resonance imaging, Contrast agent, Tumor imaging, Stimuli-responsive nanomaterials, Internal stimuli, External stimuli, Dual-mode imaging*
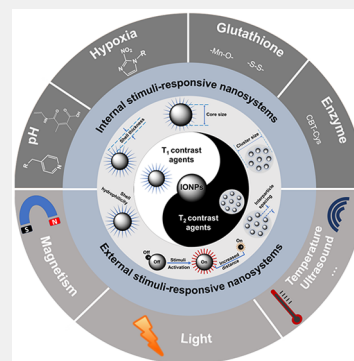
1. INTRODUCTION

Medical imaging is an important tool for disease diagnosis and monitoring. Among different imaging modalities, magnetic resonance imaging (MRI) is a well-established medical imaging method used in current routine clinical practice and is the most commonly used imaging modality for tumor evaluation.[1] MRI has the characteristics of non-invasiveness, absence of ionizing radiation, high spatiotemporal resolution, and excellent soft tissue contrast.[2-6] However, due to its low intrinsic sensitivity,[7,8] contrast agents (CAs) are required in some cases.[9] CAs can magnify the longitudinal (T_1) or transverse (T_2) relaxation rates of nearby water molecules to create tissue contrast.[10-12] T_1 CAs increase the T_1 signal intensity in T_1-weighted imaging (T_1WI), which leads to a brighter contrast enhancement, referred to as positive CAs, while T_2 CAs reduce the T_2 signal intensity in T_2-weighted imaging (T_2WI) resulting in a darker contrast enhancement, known as negative CAs.[13]

Paramagnetic gadolinium (Gd)- or manganese (Mn)-based CAs are the most common T_1 CAs in clinical use.[14] Gd-based contrast agents (GBCAs), such as Magnevist, MultiHance, Omniscan, OptiMARK, Primovist, etc., have been used widely in clinical practice.[15-18] Unfortunately, over the years, GBCAs have been related to some safety concerns, such as tissue retention of gadolinium and nephrogenic systemic fibrosis (NSF), and in some extreme cases, fractures or even death.[19-22]

Iron oxide nanoparticles (IONPs) have attracted much attention in recent years because of their unique magnetic, biocompatible, and biodegradable properties.[5,23-25] IONPs with excellent superparamagnetic performance can efficiently shorten T_2 relaxation times and may be applied as T_2 CAs for MRI.[9,26] Several formulations of IONPs (e.g., Resovist, Feridex) have received the approval of the US Food and Drug Administration (FDA) as T_2 contrast agents.[27,28] With the development of nanotechnology, the relaxation properties of IONPs can be controlled by adjusting their size, shape, and surface structure.[29,30] When the particle size is below 4 nm, ultrasmall superparamagnetic IONPs may potentially be employed to T_1 CAs.[5]

The imaging sensitivity of IONP CAs depends on their relaxivity, which is significantly dependent on the features of the IONP core properties and surface design.[26,31,32] The core properties of IONPs, including size, shape, crystal structure, and magnetic properties, occupy an important position in their contrast capacities; the related details are presented in the recent review of Gao et al.[33] Meanwhile, surface modification
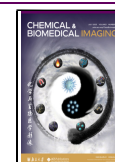
of IONPs provides a powerful toolbox to adjust their performance in MR imaging, which is a cornerstone of the so-called "smart" IONPs. Choosing different surface ligands of IONPs can enhance the accumulation of IONPs in tumor tissues and regulate the MR imaging signal. For example, specific ligands on the IONPs surface, such as antibodies, proteins, peptides, and aptamers, endow positive targeting properties, which help increase the concentration of IONPs in tumors and improve imaging sensitivity.[34−40] Moreover, surface ligands with responsive capabilities, such as pH, glutathione, enzyme, light, and so on, can alter IONP aggregation behavior and/or their hydrophilic and magnetic properties under different conditions.[41−43] Therefore, the rational design can be used to not only enhance the tumor accumulation of IONPs, but also precisely adjust the imaging signal (including the imaging mode) of the tumor, greatly enhancing the contrast of tumor images.[44,45]

In this review, we discussed the current status of different types of IONPs utilized in tumor imaging based on various external and internal stimulation. The main themes covered here are the challenges and opportunities for IONPs as MR imaging contrast agents; the structure, magnetic properties, biocompatibility, and especially the stimuli responsiveness of IONPs, as determined by their surface materials and intrinsic magnetic properties to improve MR imaging sensitivity; and the obstacles and future research directions of smart responsive IONPs.

2. DUAL-MODE MR IMAGING CONTRAST ABILITY OF IONPS

Due to their excellent safety,[46,47] good biocompatibility,[48] and facile modifiability,[32] numerous types of IONPs have been developed to explore their capabilities as tumor MRI CAs. Most importantly, the unique superparamagnetic property of IONPs endows them with advantages in both T_2WI and T_1WI. The dual-mode MR imaging contrast features of IONPs are described in the next paragraph.

2.1. Iron Oxide Nanoparticles for T_2-Weighted MR Imaging

With their specific magnetic properties, especially high saturation (Ms) values, IONPs have been used as T_2 CAs for decades. IONPs can shorten the transverse relaxation time of protons near the iron and enhance signal intensity in T_2WI. The efficiency of the transverse relaxation rate acceleration is expressed by the transverse relaxivity (r_2), which is calculated by linear fitting of the inversed T_2 relaxation times vs iron concentration. According to the quantum mechanical outer sphere theory, the main parameters affecting the r_2 value of a CA based on magnetic nanoparticles are the saturation magnetization, the effective radius, and the surface coating thickness.[49] According to the particle size, iron oxides can be classified into the three following groups: (1) ultrasmall superparamagnetic iron oxide (USPIO) nanoparticles with a particle size < 50 nm; (2) small superparamagnetic iron oxide (SPIO) nanoparticles with a particle size of 50 nm < d < 1 μm; (3) micron-sized particles of iron oxide (MPIO) with particle size above a micron.[50]

The size of IONPs greatly affects their magnetic properties and distribution in the body, thus largely determining their application.[51] For example, nanoparticles with a hydrodynamic diameter of < 5 nm could easily pass through renal filtration and discharge with urine.[52] Nanoparticles with a hydrodynamic diameter > 100 nm are rapidly cleared from the circulation by the reticuloendothelial system via active phagocytosis. Smaller nanoparticles have a relatively long half-life since they can escape phagocytosis. Consequently, optimizing the size of IONPs can avoid rapid clearance and promote accumulation in the target tissue or organ. For example, IONPs > 80 nm in diameter are efficiently captured by macrophages, which makes the size of nanoparticle suitable for imaging the reticuloendothelial system.[53,54]

The FDA has approved several commercial T_2 CAs based on IONPs for clinical applications. Ferumoxide, administrated intravenously, has been approved for liver imaging. In addition, oral ferumoxsil has been approved for gastrointestinal imaging.[50] However, the wide clinical application of these agents is limited by several drawbacks. In a transverse relaxation-weighted image, the T_2 of organizations is usually very short and decreases with the increase of field strength. Therefore, high concentrations of the CA and/or high relaxivity are needed to measure T_2.[55] Most importantly, the intrinsic dark signal produced by T_2 CAs can be confused with other low intensity areas, such as air, hemorrhage, blood clots, calcification, and metal deposition. Moreover, the phenomenon known as the "blooming effect" can distort the background image and blur the image, caused by a high magnetic moment inducing a long-distance magnetic field perturbing neighboring tissue.[56]

2.2. Iron Oxide Nanoparticles for T_1-Weighted MR Imaging

Although iron-oxide-based nanosystems are more commonly applied as T_2 MRI CAs, they have shown promise as T_1 MRI CAs in the past decade.[57] The main function of T_1 MRI CAs is to accelerate the longitudinal relaxation rates of hydrogen protons. As with the T_2 mode, the efficiency of longitudinal relaxation rate acceleration is expressed by longitudinal relaxivity (r_1), performed by linearly fitting the inverse T_1 relaxation time as a function of iron concentration. Besides the value of r_1, the ratio of r_2 to r_1 is also a critical parameter influencing a given contrast agent's ability to be used as either a T_1- or T_2-dominated MRI CA. When r_2/r_1 is > 8, the agent is suitable as a T_2 contrast agent, while when r_2/r_1 is < 5, it is suitable for T_1 imaging.[58] Therefore, creating a T_1 contrast agent involves a maximized r_1 value and a minimized r_2/r_1 value.

Depending on the Solomon-Bloembergen-Morgan (SBM) theory, the main parameters affecting the value of r_1 are the hydration number of the agent, the constant of the water exchange rate, and the rotational correlation time of the agent.[59,60] The successful design of IONP-based T_1 contrast agents is complicated, with each factor associated with inherent drawbacks. However, some key parameters that can lower the r_2/r_1 ratio have been unearthed. For example, the saturated magnetization and the r_2/r_1 value of an IONP reduce with the decrease of the size and crystallinity;[5,61−63] decreasing clustering can decrease r_2, which can also minimize r_2/r_1.[5,64] Meanwhile, previous reports have demonstrated that the hydrophilicity of the nanoparticle shell can also significantly affect the T_1 contrast effect of IONPs by influencing the water coordination of the IONP's surface and the chemical exchange of the magnetic ion.[14,45]

2.3. Limitations and Opportunities

IONPs have been widely applied as MRI CAs in medical diagnosis for primary tumors and metastases detection,[65,66] for contrast-enhanced MR angiography,[67] and for visualizing inflammatory lesions, such as atherosclerotic plaques.[68] Many

Table 1. Representative pH-Responsive Iron Oxide Nanoparticles for MR Imaging of Tumors[a]

Response	Responsive composition	Nanosystem	Relaxivity [mM^{-1} s^{-1}]				Field strength [T]	Imaging mode	Applications	Ref.
			Before stimuli		After stimuli					
			r_1	r_2	r_1	r_2				
Disassembly	2-(hexamethyleneimino)ethyl methacrylate (HMEMA)	AuNP-ESIONP vesicle	0.8	6.9	5.8	7.2	0.5	T_1-positive CA	A single r_1 increase along with a stable r_2	70
		ESIONP vesicle	0.3	53.5	5.7	5.9		T_1-T_2 dual mode CA	An r_2 decrease together with an r_1 increase	
	Dimethyl maleic amide group	ESIONP micelle	6.2	112.8	6.3	11.0		T_2-T_1 switchable CA	Selectively deactivating the T_2 contrast and enhancing the T_1 contrast.	
	Calcium carbonate (CaCO$_3$)	USPIONs@CaCO$_3$	1.3	30.0	1.2	4.8	1.5	T_2-T_1 switchable CA	Imaging of HCC	71
	Imidazole groups	PMNs	3.3	44.0	3.87	22.5		T_1-positive CA	Imaging of colon tumor	72
		NAGs	4.9	105.2	7.3	15.3	7.0	T_2-T_1 switchable CA	Imaging of breast tumor	73
	Hydrazone bonds (R-CH=N-NH$_2$)	IONAs	3.2	108	5.1	21.3	3.0	T_1-positive CA	Imaging of lung tumor	74
	I-motif DNAs	RIAs	5.2	330.3	4.3	30.7	3.0	T_2-T_1 switchable CA	Imaging of early-stage small HCC	75
Assembly	Electrostatic interaction	ESIONP	5.7	9.1	3.9	42.2	1.5	T_1-T_2 switchable CA	Imaging of breast tumor	76
	I-motif DNA	FSI$_{C5}$P	NA	R$_2 \approx$ 0.7	NA	R$_2 \approx$ 3.7	3.0	T_2-negative CA	Imaging of breast tumor	77
	Dimethyl maleic amide group	HTAMNs	0.6	98.4	0.7	88.2	3.0	T_2-negative CA	Imaging and PDT for HCCs	78
	Poly (lipid hydroperoxide)-co-poly(4-vinylpyrene) (PLHPVP)	Fe$_3$O$_4$–Au JNP	NA	445	NA	76	7.0	T_2-negative CA	Imaging and synergistic therapy of glioblastoma	79
Activation	MnO$_2$ nanosheets	Fe$_3$O$_4$@C@MnO$_2$	2.2	442.4	5.3	364	3.0	T_1-T_2 dual mode CA	Imaging of cervical cancer	80
		SPIO@SiO$_2$@MnO$_2$	1.3	13.9	4.6	82.2	3.0	T_1-T_2 dual mode CA	Imaging of breast cancer and metastatic tumor	81
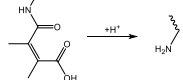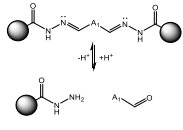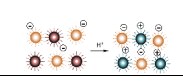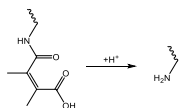
[a]Abbreviations in Table 1: hepatocellular carcinoma, HCC; contrast agent, CA; not available, NA; Photodynamic therapy, PDT.

SPIO contrast agents have been proposed, and several have already been approved by the FDA and the European Medicines Agency (EMA); however, no agent is yet available commercially.[50] After several preliminary setbacks, ferucarbotran and ferumoxide were initially introduced to the market, but later withdrawn (as better alternatives were available for the relevant diagnostic applications). In addition, several different preclinical directions are now being explored, with an increasing number of clinical applications involving the use of IONPs.[69]

With the continuous development of individualized precision medicine, people have an increasingly higher demand on specific imaging and accurate diagnosis. Increasingly, noninvasive methods, like MR imaging, can stratify patients, thus enabling the avoidance of ineffective and/or expensive, unnecessary treatments. However, the application of IONPs in personalized medicine requires high levels of sensitivity, and any single IONP cannot currently satisfy this need. The rapid development of IONP-based, stimuli-responsive MRI probes can conduct early detection, precise diagnosis, and treatment monitoring of tumors. Some of the activatable IONPs described below are expected to facilitate the progress of precision medicine.
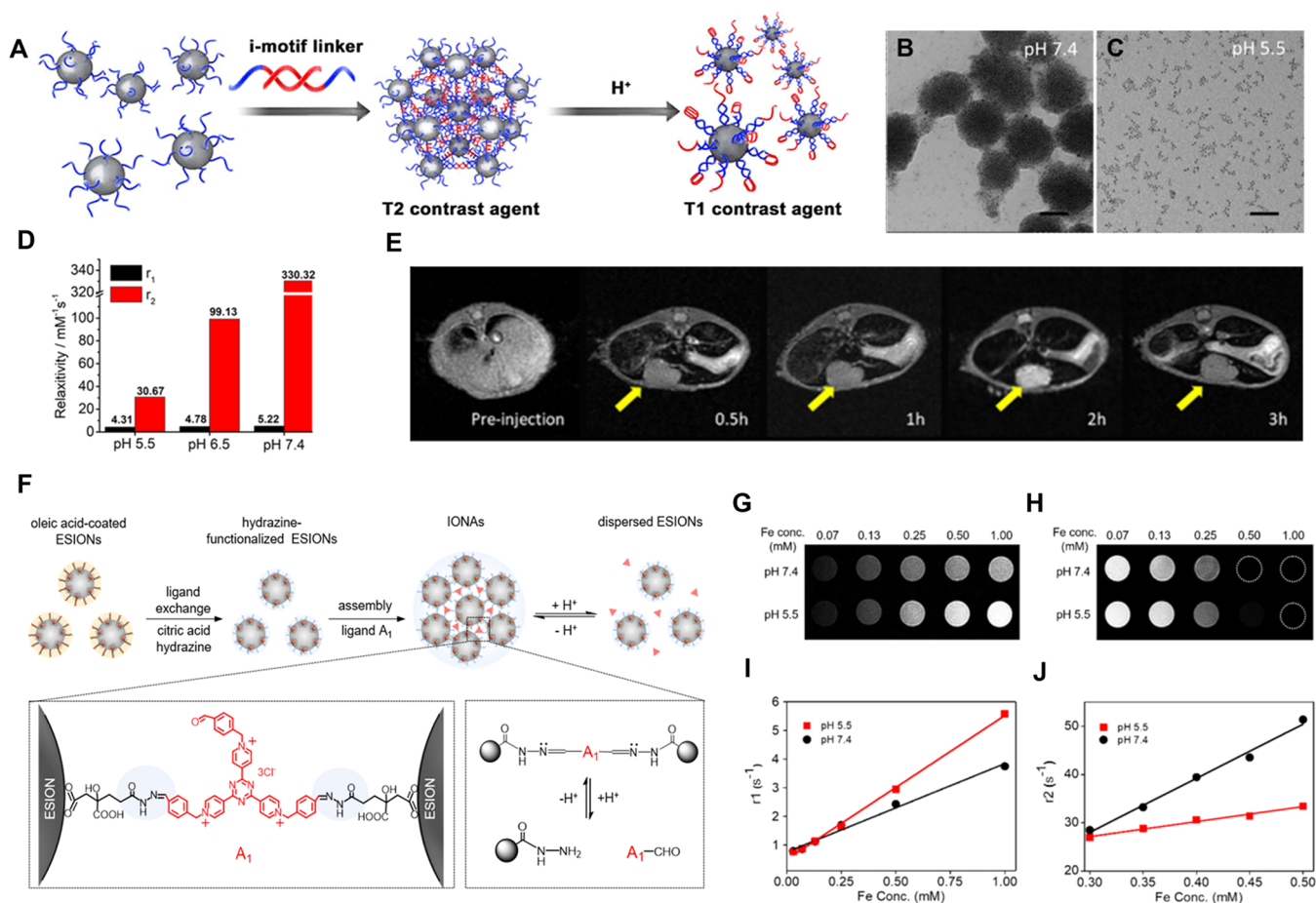
Figure 1. (A) Schematic illustration of the smart MRI CA, named RIA (pH-sensitive IONP). TEM images of RIAs at (B) pH 7.4 and (C) pH 5.5. Scale bar = 50 nm. (D) r_1 and r_2 values of RIAs at pH 7.4, 6.5, and 5.5. (E) T_1WI of RIAs in orthotopic HCC mice. Reprinted with permission from ref. 75. Copyright 2018 American Chemical Society. (F) Illustration of IONA formation and its pH-triggered disassembly. (G) T_1WI and (H) T_2WI photographs, and (I) r_1 and (J) r_2 values of IONAs at pH 7.4 and 5.5. Reprinted with permission from ref. 74. Copyright 2019 American Chemical Society.

3. DESIGNING STIMULI-RESPONSIVE IRON OXIDE NANOPARTICLES FOR TUMOR MR IMAGING

In order to overcome the disadvantages of the relatively low sensitivity and poor specificity of traditional CAs, MR CAs based on IONPs with stimuli-responsive properties have been introduced, which can respond to different physiological/pathological signals to activate the contrast signal. This section provides an overview of responsive IONPs as MRI CAs, including those responsive to internal stimuli, such as pH, hypoxia, glutathione, and enzymes, and external stimuli, such as magnetic field, light, and others.

3.1. Internal Stimuli-Responsive Iron Oxide Nanoparticles for Tumor MR Imaging

The tumor microenvironment's unique physicochemical conditions (such as pH and hypoxia) and overexpressed biomarkers (such as glutathione and specific enzymes) provide multiple targets for designing internal stimuli-responsive IONPs. The recent progress in this direction is presented below to provide the principles on which efficient MR CAs based on IONPs can be fabricated.

3.1.1. pH-Responsive IONP-Based Contrast Agents.
Tumor tissue exhibits rapid growth and metabolism, consuming large amounts of glucose and oxygen, and excessive hydrogen ions and lactate accumulate in extracellular fluids,

lowering the pH of the tumor microenvironment (pH 5.5 to 6.8).[42] As one of the earliest tumor features exploited by nanomedicines, pH-responsive strategies have been developed. A selection of representative pH-responsive IONP-based contrast agents is listed in Table 1.

Given that the relaxation properties of IONPs can be manipulated by changing their size, morphology, and surface structure, IONPs have been used as CAs for both T_1/T_2 dual-modal MR imaging for tumor diagnosis.[71,73,76] Diverse pH-responsive chemical bonds or pH-responsive degradation of some metal oxide materials provide researchers with a versatile selection.

Disassembly. pH-Triggered disassembly behavior can change the size of IONP clusters, which significantly influences their imaging signal. This strategy has been adopted by Ling and co-workers, who described an efficient method to enhance contrast in tumors by delivering assembled IONPs into tumor sites by the enhanced permeability and retention (EPR) effect of larger particles, and then decomposing them under the acidic tumor microenvironment to recover the T_1 properties of USPIO NPs.[74,75] The assembled IONPs can be absorbed by normal tissue and present a strong T_2 effect, and the disassembled particles in the tumor site have a strong T_1 effect, which improves the contrast between the tumor site and the surrounding tissue. In 2018, the same group reported an
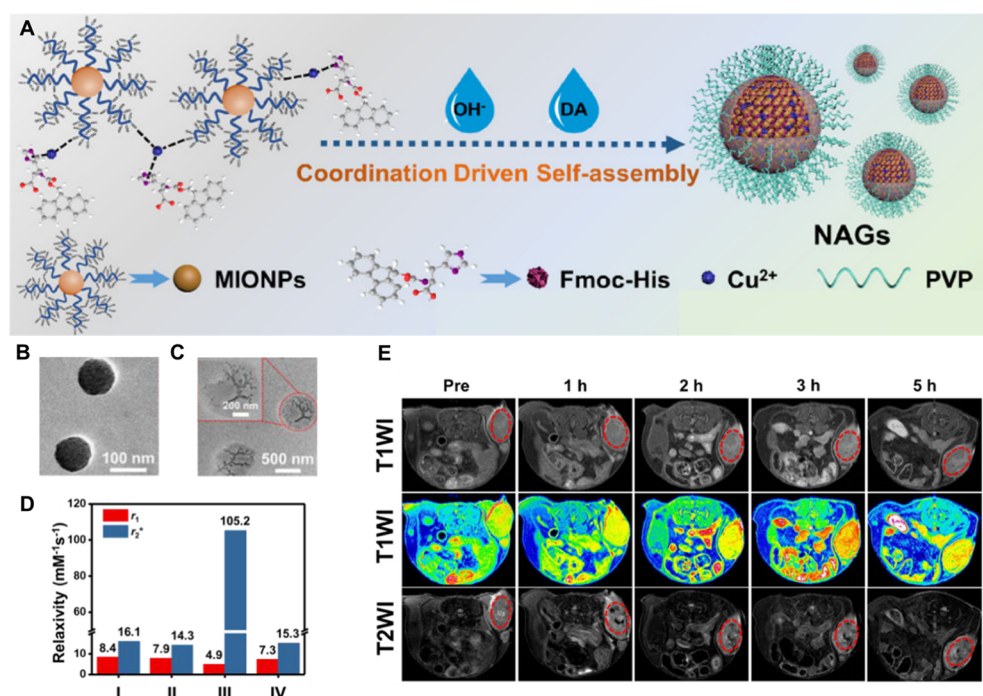
Figure 2. (A) Schematic diagram of the fabrication of NAGs. TEM images of NAGs (B) before and (C) after incubation in Tris−HCl buffers. (D) r_1 and r_2^* values of different samples. (I) IONPs, (II) IONPs at pH 6.5, (III) nanoaggregates, and (IV) disassembled nanoaggregates (Tris−HCl buffer, pH = 6.5). (E) In vivo T_1WI and T_2WI before and after intratumoral injection of NAGs. The second row shows corresponding pseudocolor T_1WI. Reprinted with permission from ref. 73. Copyright 2022 American Chemical Society.

IONP nanocluster with a pH-sensitive I-motif DNA-modified linker (RIA; Figure 1A).[75] Figure 1B and C show that the IONP nanoclusters disassemble upon encountering the acidic tumor environment, while Figure 1D demonstrates a significant drop in the r_2 relaxivity and r_2/r_1 value when the pH is acidic. This strategy greatly enhanced the T_1 MRI contrast between the normal liver and hepatocellular carcinoma (HCC) in vivo (Figure 1E), providing a highly sensitive diagnostic method for small hepatocellular carcinoma. One year later, they reported another pH-sensitive IONP nanosystem cross-linked by small-molecule ligands (IONAs; Figure 1F).[74] At pH 7.4, IONAs are structurally robust, while under the acidic conditions in tumor sites, IONAs were quickly decomposed into a large amount of hydrophilic USPIO NPs, producing a strong T_1-weighted MR signal. As shown in Figure 1G−J, the IONAs exhibited an r_1 = 3.2 $mM^{-1}s^{-1}$ and an r_2 = 108.0 $mM^{-1}s^{-1}$ at neutral pH. At a low pH value of 5.5, r_1 increased, and r_2 decreased significantly. In addition, there have been reports of other disassembling methods that regulate the signals of IONPs, including encapsulating IONPs in hydrogels[82] or polymeric micelles,[71,83] which can decompose in the acidic conditions of the tumor, and then release IONPs to enhance the T_1 contrast images of the tumor. These strategies provide a promising way to improve detection sensitivity through various ingenious designs. However, the assembled IONPs were easily sequestered in the liver by Kupffer cells due to their larger size, posing a safety risk. Therefore, the long-term metabolic effects of RIAs in the liver should be explored prior to further application.

Using the same strategy, Hou et al.[73] fabricated intelligent switchable MRI nanoprobes through coordinated self-assembly driven by IONPs. The introduction of copper ions (Cu^{2+}), which act as a linker in the microemulsion method can coordinate to the IONPs (Figure 2A). Poly(vinylpyrrolidone)

was employed to stabilize the nano aggregates of IONPs (NAGs). The nano aggregates remained aggregated under basic conditions and decomposed under acidic conditions (Figure 2B and C), resulting in a regulation of the r_1 and r_2^* (linear fitting of the $1/T_2$ vs iron concentration) values (Figure 2D). In vivo results demonstrated that these acidic-responsive nano aggregates of IONPs display a time-dependent transition from T_2 CAs to T_1 CAs at the tumor site (Figure 2E). This method helped to obtain T_1- and T_2-weighted dual-mode MR images at different time points after a single injection. Although NAGs exhibit good performance in vivo with intratumoral injection (Figure 2E), their ability to provide contrast in tumors in vivo is weaker upon venous administration. Therefore, the circulation behavior and tumor accumulation of NAGs requires further improvement.

Assembly. In contrast to the disassembling strategy, the pH-triggered assembly behavior of IONPs enlarges their aggregation size in low-pH conditions, which not only increases the accumulation and retention time of IONPs at the tumor site but also regulates the MR imaging mode from T_1-weighted to T_2-weighted. For example, Pei and colleagues[76] fabricated USPIO-based pH-responsive systems composed of USPIO NPs with different surface modifications. Under an acidic environment, USPIO NPs with different surface modifications had different surface charges, leading to assembly though electrostatic interactions between the positive and negative charges. Based on the aggregation, the T_1 contrast effect switches to a T_2 contrast effect in response to low pH. Other examples are presented in Table 1.

Activation. The degradation behavior of some metal oxide materials under acidic conditions offers multiple options for researchers to design smart IONP imaging systems. Cheon et al.[84] applied this method to establish magnetism-based nanoscale distance-dependent magnetic resonance tuning
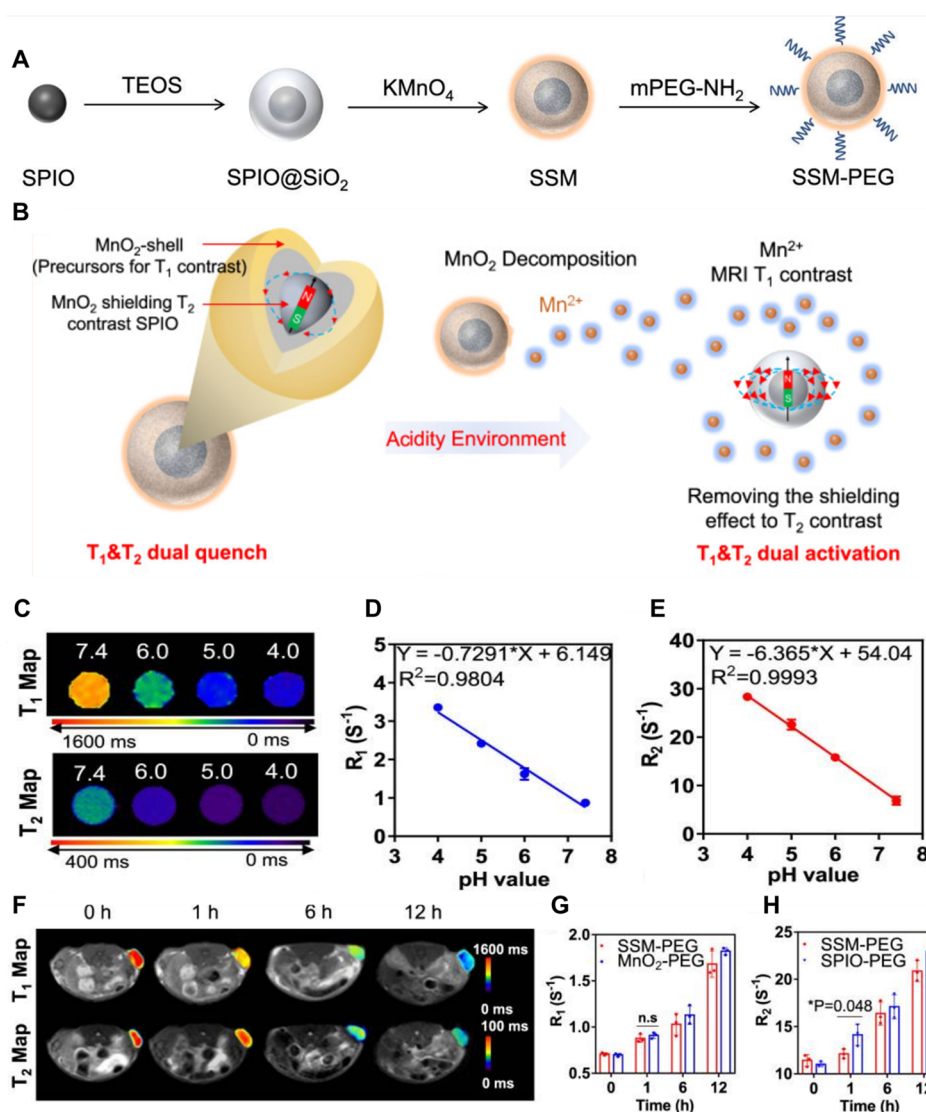
Figure 3. (A) Scheme and structure of $SPIO@SiO_2@MnO_2$ (SSM). TEOS represents tetraethyl orthosilicate. (B) $SPIO@SiO_2@MnO_2$ showed weak T_1 and T_2 contrast intensity at neutral pH, as the T_2 signal of SPIO is quenched by the MnO_2 shell. In the acidic environment, the MnO_2 layer decomposed into Mn^{2+} (T_1-weighted), and the T_1 and T_2 signals are sequentially recovered. (C) T_1 and T_2 maps of SSM in different pH environments. (D) R_1 and (E) R_2 of SSM at different pH. (F) T_1 and T_2 maps. (G) R_1 and (H) R_2 at the tumor after I.V. injection of SSM-PEG or MnO_2−PEG. Reprinted with permission from ref. 81. Copyright 2022 The Author(s).

(MRET), which is composed of a superparamagnetic quencher and a paramagnetic enhancer. In MRET, the T_1 signal intensity is suppressed by a superparamagnetic T_2 CA at a critical distance; the signal recovers when the two components separate. Using the same method, Wang et al.[81] designed and synthesized a pH-activatable T_1-T_2 dual-modal MRI CA, referred to as $SPIO@SiO_2@MnO_2$ (SSM-PEG; Figure 3A). In an acidic environment, MnO_2 decomposes into Mn^{2+}, and both T_1- and T_2-weighted signals are sequentially recovered (Figure 3B). MRI map images (Figure 3C and D) show that both R_1 (equals $1/T_1$) and R_2 (equals $1/T_2$) values decrease as the pH value decreases. In vivo results further demonstrated that the values of T_1 signal intensity were similar for the MnO_2 and SSM groups at the tumor sites, while SSM displayed a visibly lower T_2 contrast in the first hour; until 12 h postinjection, SSM and SPIO demonstrated a similar T_2 contrast signal (Figure 3F−H). Importantly, the release of Mn^{2+} from tumor tissues may pose a safety risk to healthy

tissues or organs. Therefore, the metabolism of SSM-PEG in vivo and other aspects of safety should be examined.

3.1.2. Hypoxia-Responsive IONP-Based Contrast Agents. Hypoxia regulates tumor growth and impacts the therapeutic effect of drugs.[85] Thus, it is important to analyze the distribution and degree of tumor hypoxia in patients to facilitate individualized treatment strategies.[86] As discussed above, the size of IONPS is conducive to the penetration effect and MRI enhancement, thus making IONPs promising agents for hypoxia-responsive imaging.

Assembly. Due to their selective bioreductive feature in hypoxic tissues, nitroimidazole compounds have been widely employed for hypoxia imaging.[87−89] For example, Filippi et al.[87] developed a hypoxia-specific T_2 CA by conjugating 10-nm-sized IONPs with oxygen-sensitive metronidazole ligands, showing selective accumulation of the nanoparticles in hypoxic two- and three-dimensional cell models. In addition, our research team[88] amplified tumor imaging signals using a novel USPIO self-assembly (UIO-Pimo), possessing nitroimidazole
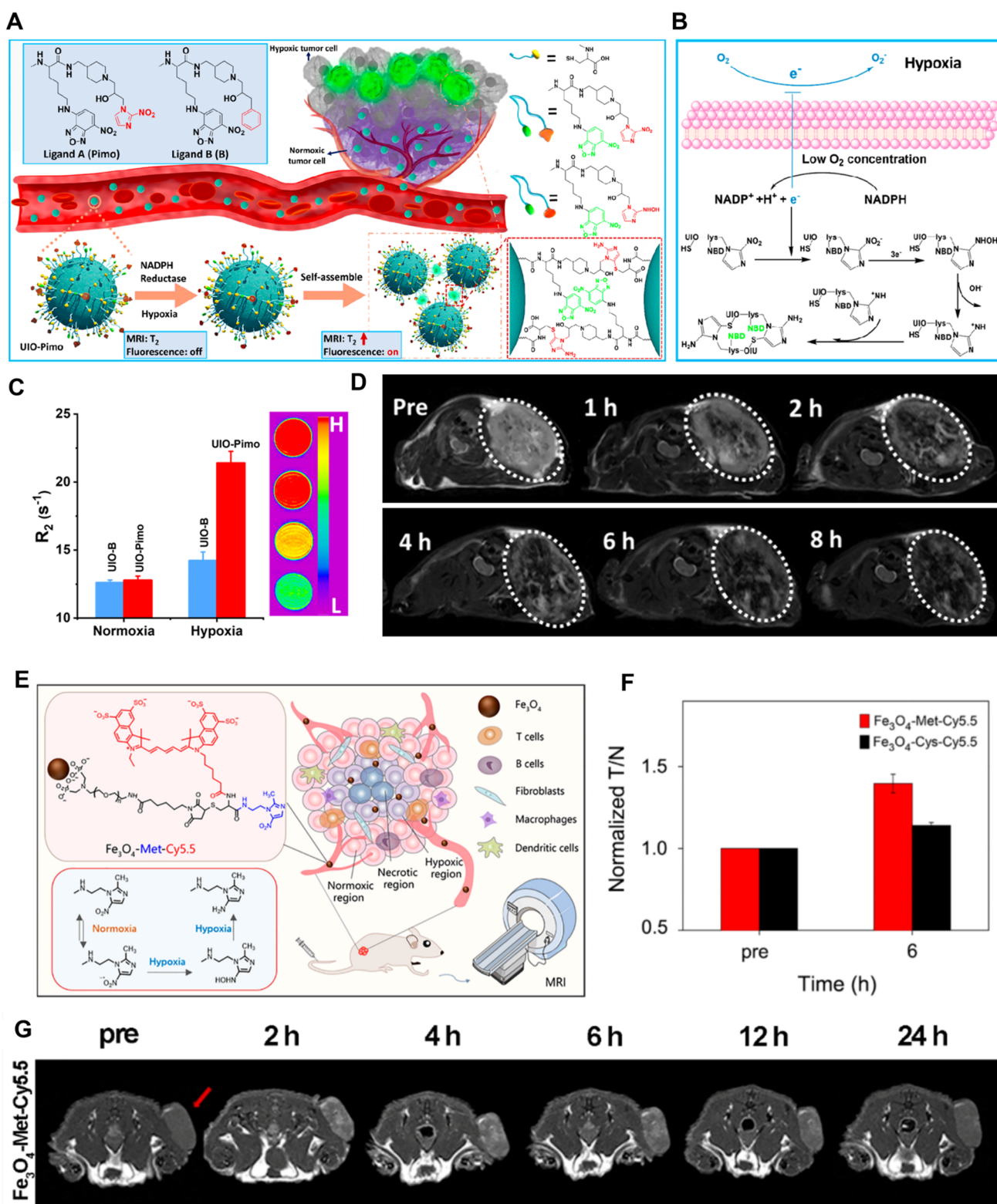
Figure 4. (A) Schematic illustration of the USPIO NPs self-assembly under hypoxia environment, which magnified the signal of MRI and fluorescence. (B) Illustration of the UIO-Pimo self-assembly under hypoxic conditions. (C) Relaxation values of UIO-Pimo and UIO-B under normoxia and hypoxia. (D) T_2WI of tumor after intravenous injection of UIO-Pimo. Reprinted with permission from ref. 88. Copyright 2021 American Chemical Society. (E) Schematic of the Fe_3O_4-Met-Cy5.5 nanoprobe for in vivo T_1WI and the mechanism of the trapping of metronidazole in hypoxic regions. (F) MRI signals before and after injection of two nanoprobes. (G) T_1WI of tumor-bearing mice within 24 h after injection with Fe_3O_4-Met-Cy5.5. Reprinted with permission from ref. 89. Copyright 2022 The Author(s).

derivatives (Pimo) on their surface as the hypoxic trigger (Figure 4A). The ultrasmall size of UIO-Pimo promotes the penetration of nanoparticles into the hypoxic region of the

tumor (Figure 4B), while the intermolecular cross-linking between Pimo and thiol group induces the irreversible aggregation of UIONPs under hypoxia, enhancing the T_2

Table 2. Representative GSH-Responsive Iron Oxide Nanoparticles for Tumor MR Imaging[a]

Response	Responsive composition	Nanosystems	Relaxivity [mM⁻¹ s⁻¹] Before stimuli r_1	r_2	After stimuli r_1	r_2	Field strength [T]	Imaging mode	Applications	Ref.
Disassembly	disulfide bonds $R_1\!-\!S\!-\!S\!-\!R_2 \xrightarrow{GSH} R_1\!-\!SH + HS\!-\!R_2$	ICNs-RGD	5.5	103.0	7.4	14.3	0.5	T_1 positive CA	Precise diagnosis of malignant gliomas	93
		Ultra-small Fe₃O₄ NPs	32.3	62.4	18.5	133.8	0.5	T_2-T_1 switchable CA	Imaging of breast tumor	94
		Fe₃O₄ nanoclusters	1.4	26.4	3.9	9.0	3.0	T_2-T_1 switchable CA	Imaging of breast tumor	95
		USD complexes	0.2	37.4	2.7	26.3	7.0	T_1 positive CA	Imaging and treatment of colon cancer	96
		AuNWs	1.1	37.4	3.2	26.3	7.0	T_1 positive CA	Imaging and PTT for malignant gliomas	97
	copper ions	MNSs@IR-780	1.6 times higher of T_1 signal intensity than control				3.0	T_1 positive CA	Imaging of gastric carcinoma and as theragnostic agents	98
Assembly	nucleophilic cysteinyl residue	HIONPs	r_2/r_1= 3.0		r_2/r_1= 6.0		0.5	T_1-T_2 dual mode CA	Imaging of liver metastasis ultra-sensitively	99
	Hydrophilic change	SIONPs	NA	177.3	NA	323.9	3.0	T_2 negative CA	Differential diagnosis between inflammatory mass and malignant glioma	100
	disulfide bond and maleimide moieties	99mTc-labeled Fe₃O₄ NPs	NA	1.2	NA	>2.18	3.0	T_2 negative CA	Imaging of colon adenocarcinoma	101
		NP-S-S-Pep	ΔR_1 = -24% , ΔR_2 =36%				7.0	T_1-T_2 dual mode CA	Imaging the spatial heterogeneity of GSH within the brain gliomas	102
Activation	Mn₃O₄ shell	RANS	2.4	92.2	16.1	258.6	1.5	T_1-T_2 dual mode CA	Imaging of gastric carcinoma as T_1 and T_2 CAs	103
	disulfide bonds	Fe₃O₄-SS-Gd₂O₃	5.6	NA	16.0	NA	3.0	T_1 positive CA	Imaging of renal carcinoma cells	104
		DCM@P-Mn-SPIO	1.2	11.7	5.2	88.8	7.0	T_1-T_2 dual mode CA	Imaging of prostatic cancer	105
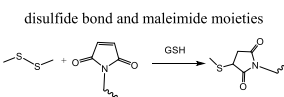
[a]Abbreviations in Table 2: contrast agent, CA; photothermal therapy, PTT; not available, NA; signal-to-noise ratios, SNR.

imaging signal there (Figure 4C and D). Additionally, the bioreductive property of nitroimidazole also provide a hypoxia-targeting ability to improve the MR imaging signal in the tumor. For example, Yang et al.[89] synthesized a hypoxia-sensitive T_1 CA (Fe₃O₄-Met-Cy5.5) by conjugating a metronidazole ligand and cyanine (Cy) 5.5 dye onto the surface of USPIO NPs (Figure 4E); the in vivo results demonstrated a significantly enhanced signal contrast intensity at the tumor site compared with controls (Figure 4F and G). This study validated that the cell uptake behavior of Fe₃O₄-Met-Cy5.5 in hypoxic conditions was consistent with the increase in cellular HIF-1α expression levels. However, validation in animal models is still needed to confirm the tumor accumulation behavior of Fe₃O₄-Met-Cy5.5.

Hypoxic imaging is a promising research direction in nanomedicine for its significance in tumor diagnosis and therapy. However, few hypoxia-responsive IONPs have been developed to explore this application in MR imaging; additional studies are expected in the future.

3.1.3. GSH-Responsive IONP-Based Contrast Agents.
During the process of tumor growth, reactive oxygen species (ROS) are produced within the cell. In response to the elevated oxidative stress in their environment, tumor cells synchronously increase the production of reducing substances, such as glutathione (GSH).[90,91] It has been reported that the concentration of GSH in most tumor cells is significantly higher than that in normal cells, making the feature a unique biomarker for designing precise tumor contrast agents.[92] A

selection of representative GSH-responsive IONP-based contrast agents is listed in Table 2.

Disassembly. The breaking of GSH-sensitive chemical bonds can lead to the decomposition of IONP clusters, which significantly influences their imaging signal. Cao et al.[93] constructed USPIO NPs encapsulated in disulfide-cross-linked poly nanogels. Through the stimuli-responsiveness to GSH, the clustered IONPs were converted into dispersed nanoparticles, completing the switching from a T_2 CA to a T_1 CA, thus realizing the selective amplification of the T_1 signal intensity.

Assembly. Simple clustering of IONPs within the tissue can increase T_2 enhancement. Depending on this, Wu et al.[100] developed GSH-sensitive IONPs (SIONPs) for noninvasive imaging differential diagnosis for gliomas, composed of an amphiphilic GSH-sensitive polymer as the surface ligand and oleic-acid-modified IONPs as the magnetic core (Figure 5A). Upon exposure to the tumor microenvironment, the disulfide linkages are cleaved by GSH and induce the aggregation of IONPs (Figure 5B and C), increasing the r_2 value (Figure 5D). In vivo results demonstrate that, compared with the MR images of inflammatory tissue, SIONPs were able to provide selective contrast enhancement of the reductive microenvironment in tumors (Figure 5E). It is important to note that the aggregation behavior of SIONPs is not easily observed by TEM images or Prussian blue staining of the tumor tissue. Synchrotron radiation methods, based on the iron element,
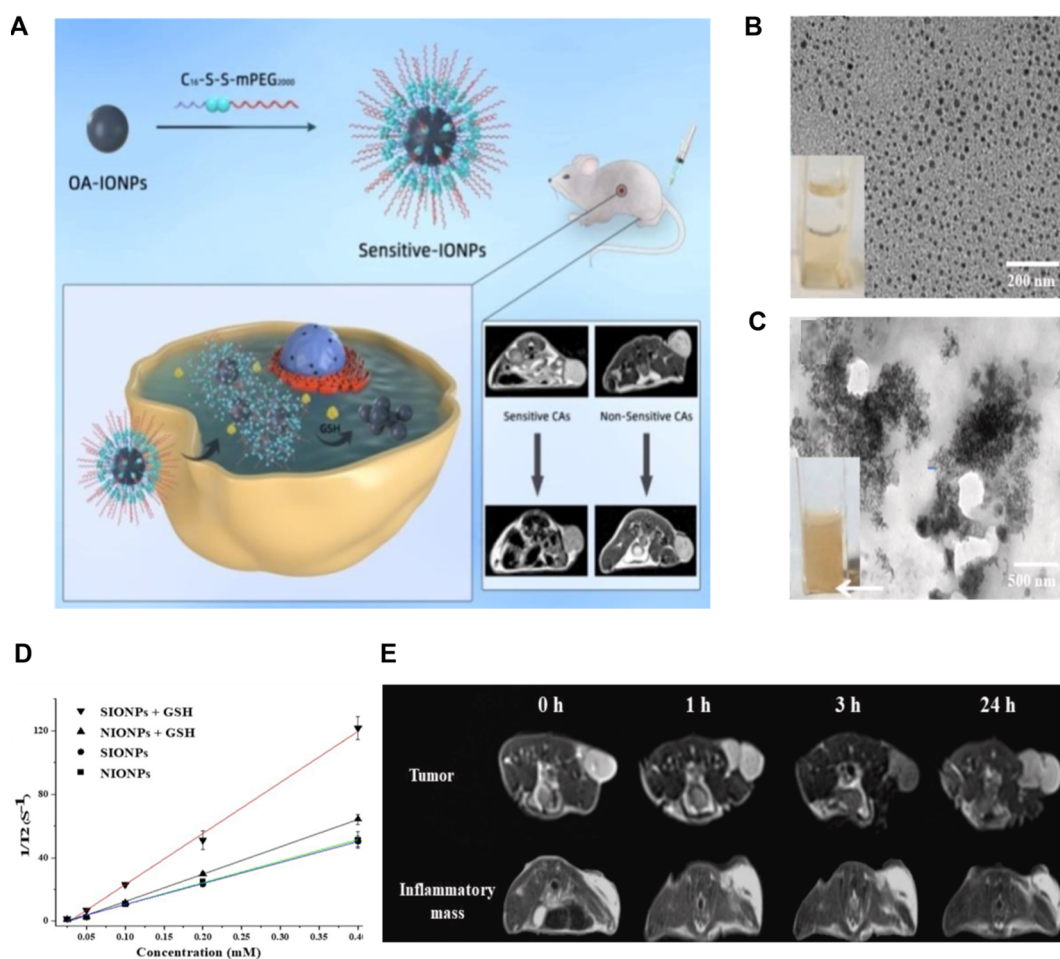
Figure 5. (A) Illustration of the preparation of GSH-activated MRI probe SIONPs. TEM images of SIONPs (B) before and (C) after incubation with GSH. The inset photograph shows that the clear hydrophilic SIONPs solution became turbid in response to GSH, forming evident precipitation. (D) Graphs of $1/T_2$ against the Fe concentration for different groups. (E) In vivo T_2WI of a tumor and an inflammatory mass at the indicated times post-I.V. injection of SIONPs. Reprinted with permission from ref. 100. Copyright 2021 Elsevier Ltd.

developed by our research group may be a promising strategy.[106]

In 2017, Gao and co-workers[101] constructed a GSH-induced in situ cross-linking reaction to assemble IONPs in tumor sites, resulting in a remarkable enhancement of T_2 imaging. In 2021, using a similar approach, the authors developed another GSH-responsive IONP imaging probe (NP−S−S−Pep) for the detection of a small intracranial tumor (Figure 6A).[102] Maleimide surface residues were introduced in order to react with the thiol group in the peptide sequence, which was produced by a reduced disulfide bond with GSH. The click reaction was able to effectively induce the Fe_3O_4 nanoparticles to aggregate in the presence of GSH. Upon exposure to GSH, the ΔR_1 ($R_{1post} - R_{1pre}$) of the nanoplatforms quickly decreases, with $\Delta R_2/\Delta R_1$ quickly increasing, while ΔR_2 ($R_{2post} - R_{2pre}$) behavior is the mirror opposite of that of ΔR_1 (Figure 6B and C). Similarly, ΔR_1 decreases with an increase in GSH concentration, while ΔR_2 shows the opposite trend (Figure 6D). In vivo results of this work also demonstrate that the responsive NP−S−S−Pep probe responded to GSH, resulting in opposite tendencies in T_1 and T_2 signal variations after the injection (Figure 6E). The activity of maleimide requires the Pep to maintain a high degree of shielding; whether this remains stable in the blood requires further confirmation.

IONPs can also be employed for the detection of metastases. Liver metastases (LM) occur in a variety of malignancies, and early accurate diagnosis is crucial for improving the prognosis.[107] However, there are no effective approaches to achieve an early diagnosis of small LMs. Xu et al.[99] developed a GSH-responsive hyaluronic-acid-coated IONP (HIONP), which is used for highly sensitivity diagnosis of LMs (Figure 7A). The covered HA can be swapped by GSH, causing unstable and aggregation of IONPs. The high GSH led to the accumulation and gathering of IONPs, reducing the T_2 signal intensity in the liver (Figure 7C). In contrast, HIONPs entering metastatic tumors increased the T_1 signal intensity in the tumors (Figure 7B). Thus, contrast-enhanced MRI by HIONPs can distinguish metastases (bright, Figure 7D) and peripheral normal liver tissues (dark, Figure 7D). However, not all types of metastatic lesions exhibit lower GSH levels than normal liver tissue, which limits the broad application of HIONPs.

Activation. The T_2 signal of IONPs can quench the T_1 relaxivity of Gd chelates.[108] Accordingly, Li et al.[104] developed an activatable MRI nanoprobe (Figure 8A) for tumor cell recognition in the presence of GSH. The cleavage of a disulfide bond by GSH between IONPs and PEG-coated gadolinium oxide (PEG-Gd_2O_3) NPs lightened the T_1 signal of PEG-Gd_2O_3 (Figure 8B). Such T_1 signal enhancement was shown to
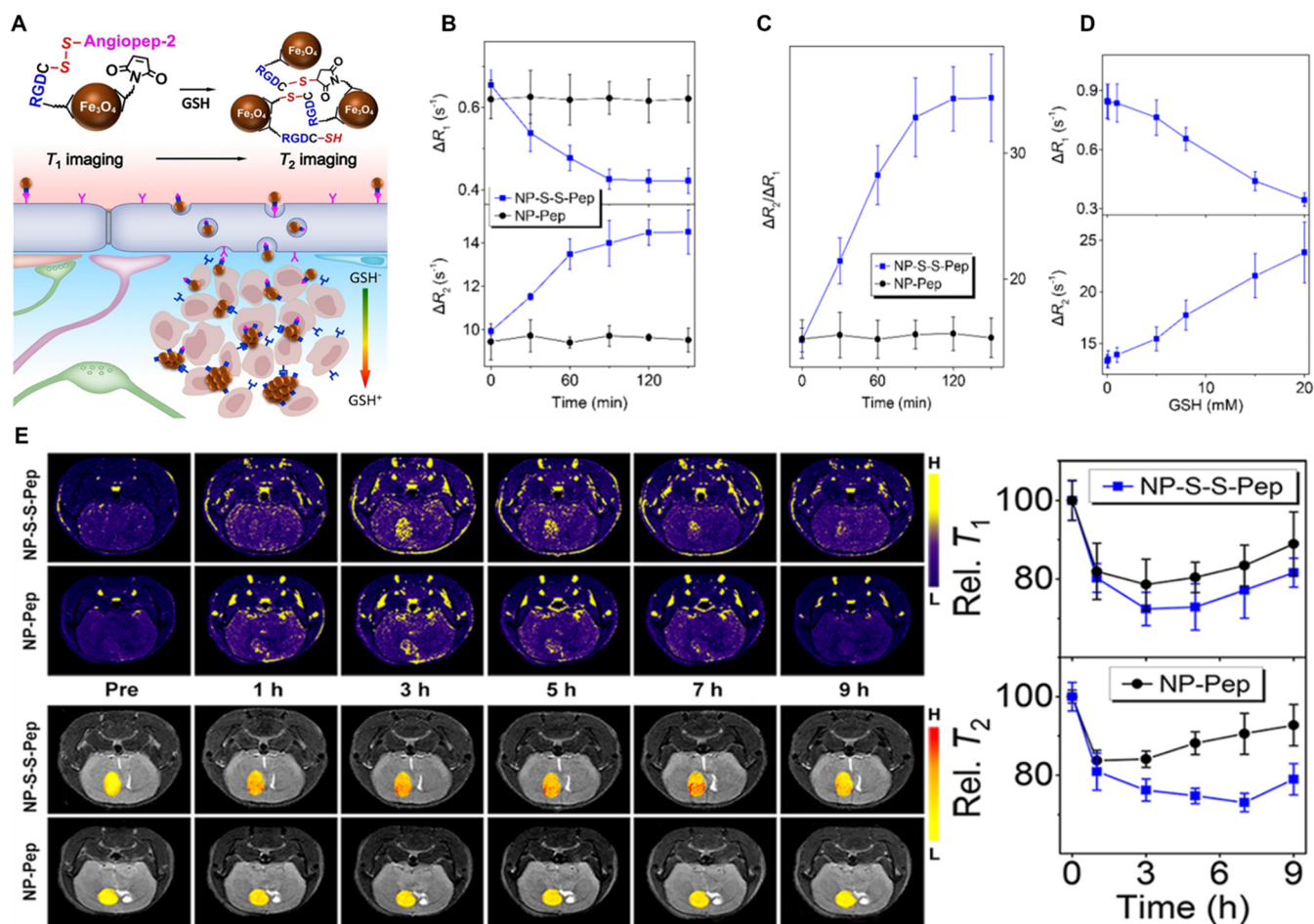
Figure 6. (A) Illustration of the molecular mechanism of GSH-induced aggregation of the smart probe. Temporal evolutions of (B) ΔR_1 and ΔR_2 and (C) $\Delta R_2/\Delta R_1$ for the GSH-responsive and nonresponsive IONPs during incubation with GSH. (D) GSH concentration dependence of ΔR_1 and ΔR_2 for the GSH-responsive IONP. (E) T_1WI (top) and T_2WI (bottom) of brain glioma after intravenous injection of different probes, respectively, with the corresponding T_1 and T_2 signals on the right. Reprinted with permission from ref. 102. Copyright 2021 Wiley-VCH GmbH.

be highly selective for GSH. Although the in vitro performance of these nanoprobes is favorable, further investigation is required to confirm their utility in vivo.

The dense T_1 CA shell may also limit the T_2 relaxation of IONPs. Therefore, Kim et al.[103] developed a T_1/T_2 dual mode recovery imaging nanoprobe by wrapping IONPs with a GSH-responsive paramagnetic Mn_3O_4 nanoshell (RANs; Figure 8C). After activation in a GSH solution, NPs exhibited stronger T_1 contrast enhancement than that in water (Figure 8D and F). Moreover, an apparent darkening contrast effect in the T_2WI was observed (Figure 8E and G). Furthermore, the group's in vivo results demonstrate a positive signal enhancement in T_1WI and a negative signal enhancement in T_2WI in the tumor sites (Figure 8H and I). Obvious cell death (survival below 50%) from RANs was observed at 14 $\mu g_{metal}\cdot mL^{-1}$. Thus, the safety of RANS will require careful consideration.

Quantitative analysis of GSH concentrations within tumors is of interest. Li and colleagues[105] recently reported an intriguing T_1/T_2 dual modality MRI probe constructed by enveloping two-way MRET pairs (TMRET), consisting of a Mn^{2+} chelate and SPIO NPs, which disintegrated and released the disassociated pairs by GSH (Figure 9A). The Mn^{2+} is both an "enhancer" in the T_1WI and a "quencher" in the T_2WI, whereas the SPIO NP is an "enhancer" in the T_2WI and a "quencher" in the T_1WI. For this nanoprobe, T_1WI and a

color-coded T_1 map revealed apparent T_1-activatable effects upon exposure to GSH (Figure 9B). A similar T_2-enhancement phenomenon was also observed in T_2WI and T_2 maps (Figure 9C). The T_1 and T_2 mapping images indicated quantitative MRI visualization of GSH in the tumor (Figure 9D). Also, both ΔR_1 and ΔR_2 were positively related to the concentration of GSH in vivo (Figure 9E and F), which can visualize and quantify molecular targets noninvasively. It is important to note that the synthetic route of DCM@P−Mn−SPIO involved complex synthesis and functionalization steps, which pose a challenge in large-scale synthesis. Therefore, it will be necessary to further simplify the synthetic process for successful clinical translation of this strategy.

3.1.4. Enzyme-Responsive IONP-Based Contrast Agents.
Specific enzymes can be upregulated upon the onset of a pathological condition, making such proteins potential imaging targets. Therefore, responsive IONP probes can be designed to possess surface moieties that become modified under the action of specific enzymes, resulting in substantially different relaxivity values.

Disassembly. Some enzymes can trigger the disassembly of IONPs clusters, enhancing imaging signal intensity. For example, Guo et al.[109] developed coacervate nanoprobes with a trypsin-responsive near-infrared fluorescence (NIRF)/MR
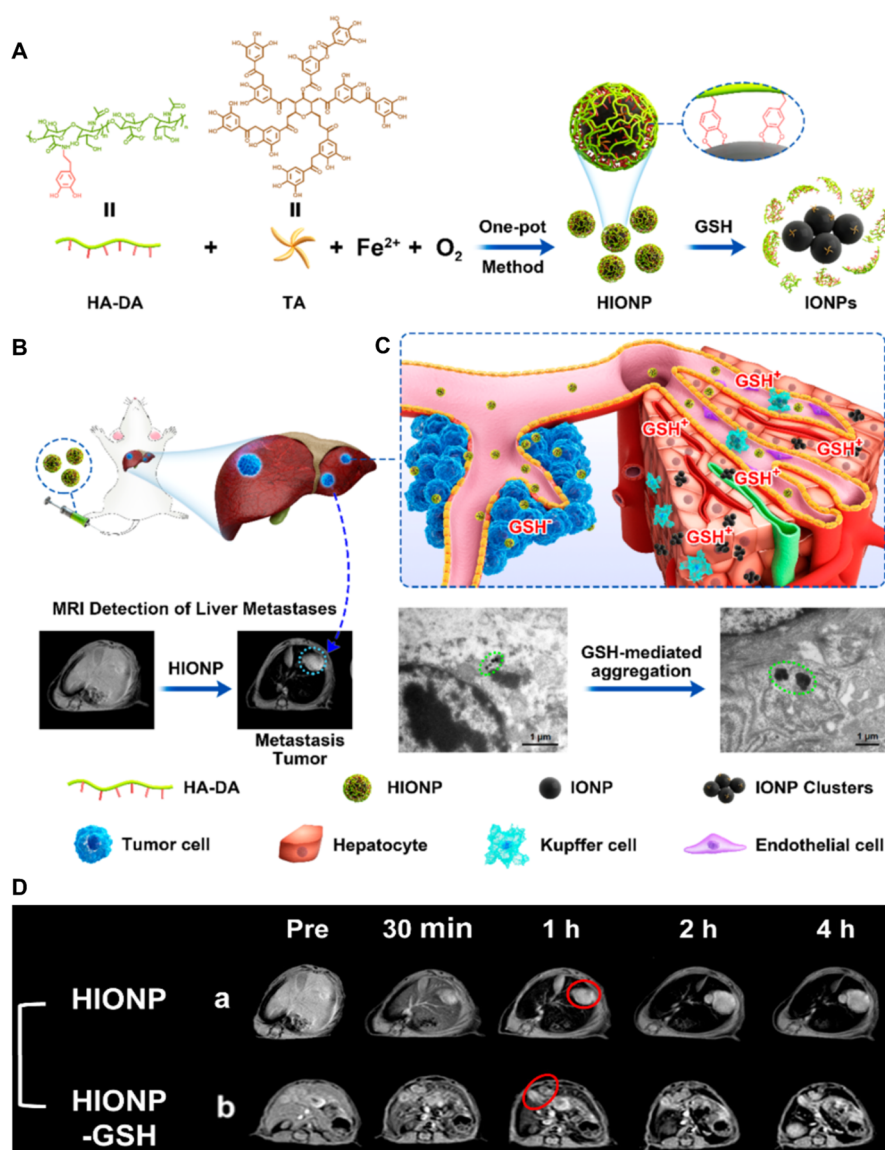
Figure 7. (A) Illustration of the fabrication of HIONPs, and the GSH-responsive agglomeration. (B) Illustration of GSH-responsive HIONPs with high sensitivity diagnosis of liver metastases, and (C) the transformation of HIONPs in metastases (nonaggregation) and normal liver (aggregation). (D) T_1WI of B16F10 liver metastases injected with HIONPs, and HIONPs pretreated with diethyl maleate. Representative metastases are indicated by red circles. Reprinted with permission from ref. 99. Copyright 2021 American Chemical Society.

dual imaging ability to enhance the diagnostic sensitivity of tumors.

Assembly. Enzymes can change IONP surface properties, promoting polymerization or dissociation of IONPs, thus changing the T_2 relaxation efficiency of IONPs. Based on the aggregation-enhanced T_2 effect of IONPs, Long et al.[110] designed a response strategy (Figure 10A) that exploits the increase of r_2 after the aggregation of IONPs. The authors synthesized two sets of IONPs, which selectively performed a copper-free click reaction upon exposure to matrix metalloproteinase (MMP) enzymes to form self-assembled aggregates.

Similarly, in 2016, Liang and co-workers[111] designed an enzyme−stimuli IONP system, characterized by caspase3 (Casp3)-induced aggregation, which can be applied for T_2 contrast enhancement of tumor apoptosis (Figure 10B). The authors developed a small molecule and modified it onto the surface of USPIO NPs to fabricate the responsive IONPs

system (Fe$_3$O$_4$@1 NPs). Figure 10C and D demonstrated that IONP aggregates were realized in vitro in the presence of Casp3/7 and in the apoptotic HepG2 cells that exhibit high expression of Casp3/7 (Figure 10E). Meanwhile, the r_2 value of the apoptotic cells with Fe$_3$O$_4$@1 NPs was the highest of all groups (Figure 10F). In vivo results demonstrated that the Fe$_3$O$_4$@1 NPs is specific to tumor apoptosis in T_2 contrast enhanced MRI (Figure 10G). In 2020, the same group described the fabrication of furin-instructed self-aggregating IONPs, via a CBT-Cys click condensation reaction for enhanced MR T_2 imaging to accurately guide the photothermal therapy.[112] The improved performance of T_2-weighted imaging in that work comes from the enhancement of IONP concentration and the aggregation behavior of the IONPs. A mechanism to distinguish the contribution of each effect in vivo remains unclear, and novel characterization methods are needed.
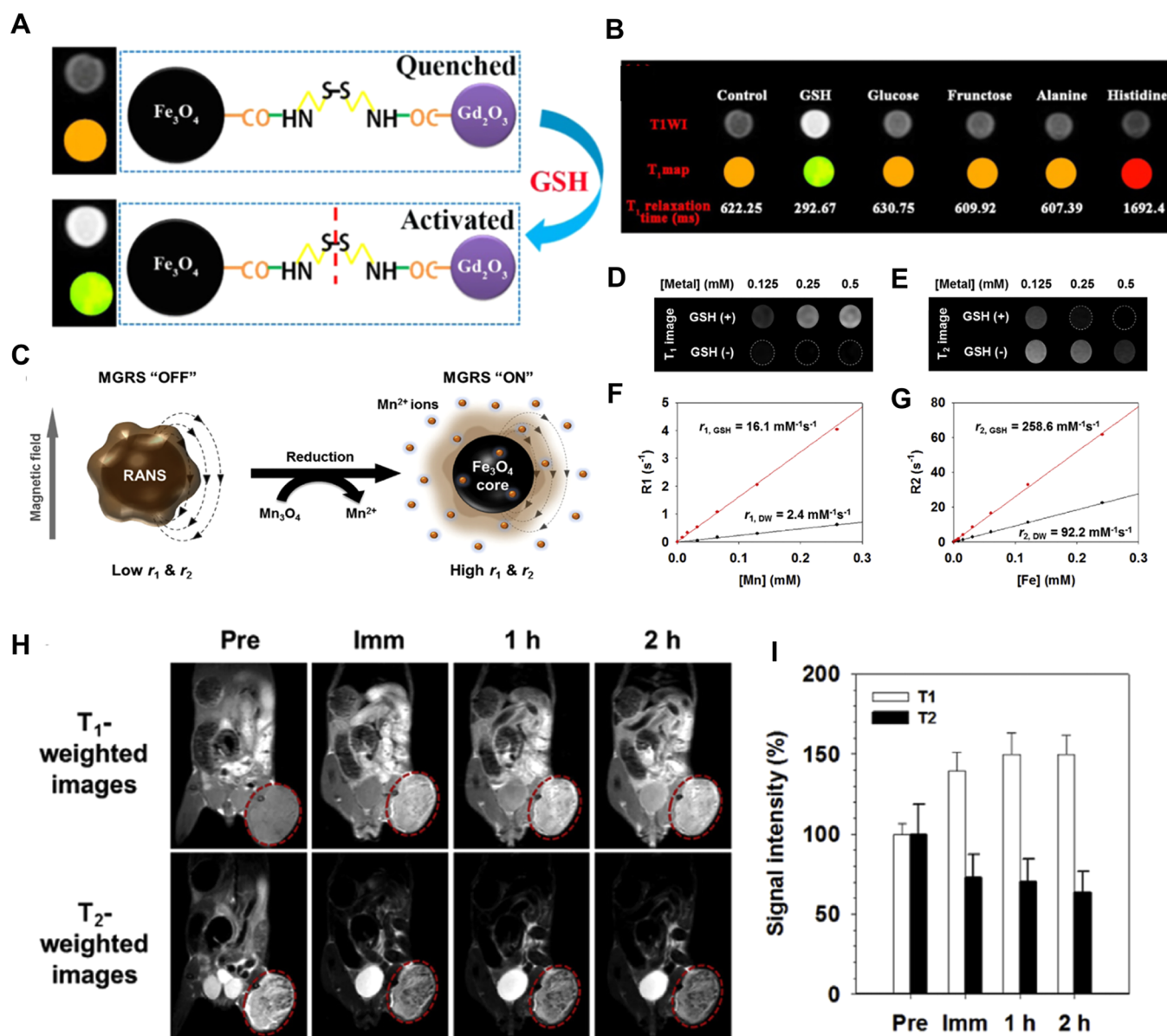
Figure 8. (A) Illustration of the fabrication of the GSH-responsive nanocomplex ($Fe_3O_4-SS-Gd_2O_3$). (B) T_1WI, T_1-map images, and the corresponding T_1 relaxation time of the $Fe_3O_4-SS-Gd_2O_3$ nanocomplex in different environments. Reprinted with permission from ref. 104. Copyright 2016 Elsevier B.V. (C) Illustration of the GSH-responsive activatable nanoshell. (D) T_1WI and (E) T_2WI of the nanosystem after incubation with or without GSH. Relaxivity plots of (F) T_1 and (G) T_2 relaxation rate analyses. (H) In vivo T_1WI and T_2WI of MKN-45 tumor-bearing mice taken before and after intravenous injection of the redox-responsive activatable nanoshell. (I) Relative T_1 and T_2 signal intensities (%) of tumor sites at the indicated time points. Reprinted with permission from ref. 103. Copyright 2016 Elsevier Ltd.

Activation. As discussed above, upon conjugation to IONPs, the T_1 relaxation signal of Gd chelates can be quenched.[113] Using this strategy, Gao et al.[114] designed novel NP-bioconjugates ($Fe_3O_4-pepA-Gd$) by conjugating Gd chelates and IONPs with an MMP-2 cleaved linker as MRI CAs, which achieve T_1 relaxivity recovery (Figure 11A). This bioresponsive linker was successfully cleaved by MMP-2, causing the Gd chelate to be released from the nanosystem. Subsequently, the T_1 signal produced by the Gd chelate recovered over time (Figure 11B). In vitro results demonstrated that the T_1 decreased by 2.5-fold and the T_1WI became bright, with the contrast from the bioresponsive IONPs (Figure 11C). The tumor area became bright with $Fe_3O_4-pepA-Gd$ contrast enhanced T_1 sequences in vivo (Figure 11D), while the control probe had no signal enhancement in

the tumor area (Figure 11E). However, this work only investigated the T_1 relaxivity recovery due to the release of Gd chelates from $Fe_3O_4-pepA-Gd$, and did not evaluate the T_2 relaxivity recovery of central superparamagnetic Fe_3O_4 nanocrystals, which could be further investigated.

As the disorders of enzymes are obvious in different types and different stages of tumors,[115] it is necessary to personalize nanoparticles based on specific tumor subtypes and stages, and consider diverse diseases or physical conditions of the patient. Furthermore, the liver contains large amounts of hydrolases, which may cause the enzyme-responsive nanoprobe to lose the ability to respond in the tumor site, and should also be considered in the design of enzyme-responsive IONP systems.[116]
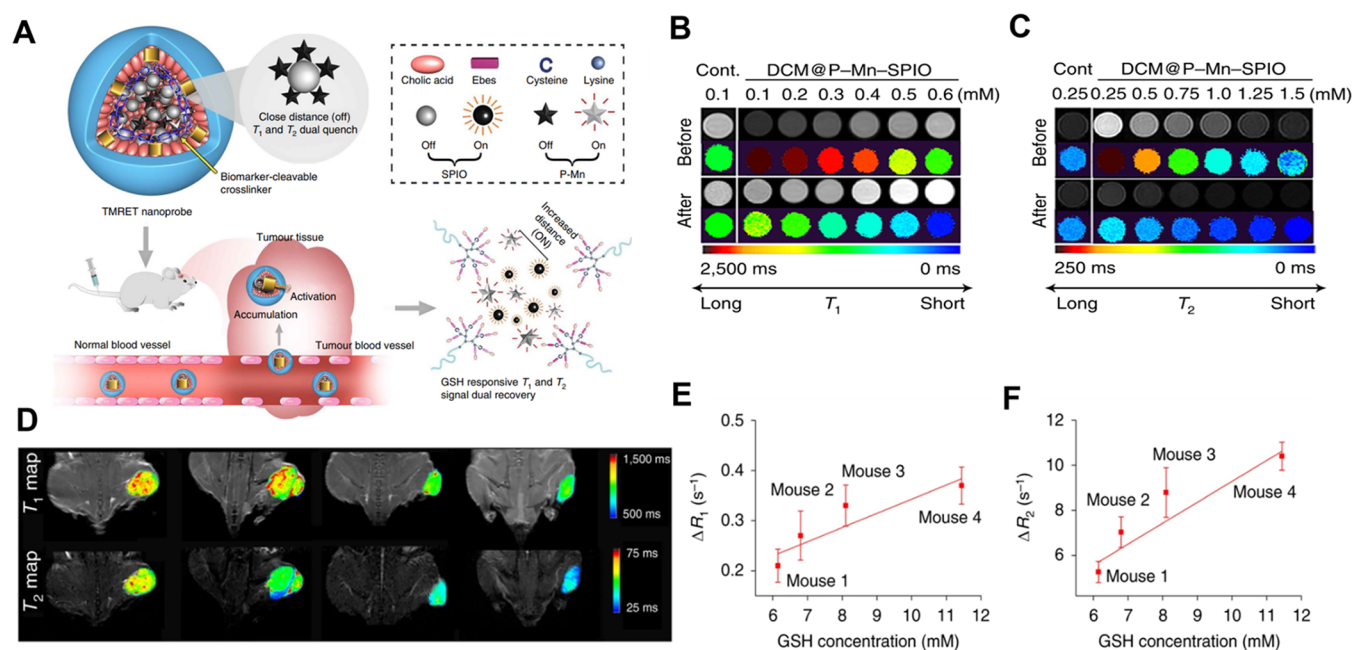
Figure 9. (A) Schematic illustration of the two-way magnetic resonance tuning (TMRET) nanotechnology. (B) T_1WI and the color-coded T_1 map and (C) T_2WI and the color-coded T_2 map of DCM@P−Mn−SPIO before and after incubation with GSH. (D) Quantitative MRI visualization of GSH in tumors by DCM@P−Mn−SPIO. Plots of (E) ΔR_1 and (F) ΔR_2 of the tumors versus tumor GSH concentration. Reprinted with permission from ref. 105. Copyright 2020 The Author(s), under exclusive license to Springer Nature Limited.

3.1.5. Multiple Internal-Responsive IONP-Based Contrast Agents. Multiple-responsive IONPs respond to two or more different internal factors.[117,118] This strategy may overcome the shortcomings of a single responsive approach, provide a more accurate signal-regulated feature of the tumor, and avoid the generation of false images, which can affect the clinician's judgment.

Disassembly. Such multiresponsive IONPs are stable in a single condition but sensitive to multiple conditions at the tumor site. For example, Li et al.[119] constructed a T_2-T_1 switchable IONP with a pH/H_2O_2 dual-responsive ability (Figure 12A). The assembled USPIO NPs can be used as CAs for T_2-weighted MR imaging. When the assembled probe was exposed to the elevated H^+ and H_2O_2 concentrations within the tumor, the nanoparticles were dissociated and redispersed into USPIO NPs, leading to the T_2 MRI signal converting to a T_1 MRI signal (Figure 12B). In vivo results further showed a strong T_2 imaging signal (SNR [signal-to-noise ratio] = 0.5) at tumor site after 2 h post-injection with the dual-responsive IONPs. Over time, the imaging signal has gradually transformed into a T_1 signal, reaching a maximum at 8 h (Figure 12C). The concentrations of the USPIO NPs in the liver and spleen were greater than that in the tumor tissue until 21 d. Therefore, strategies to decrease the accumulation of USPIO NPs in normal tissue should be an important direction of future work. Sometimes, multiple-responsive IONPs need to respond to different conditions sequentially. For instance, Song et al.[120] constructed smart nanoplatforms, which possessed the ATP responsiveness and pH-facilitated decomposition behavior, eliciting a remarkable change in transverse relaxivity.

Assembly. In 2017, our group reported USPIO NPs with hyaluronic acid (Fe_3O_4@HA) as a surface modification to tune the T_1 and T_2 signal intensity by aggregating via degrading HA to exposure to hyaluronidase (HAase) and an acidic environment (Figure 12D).[121] The T_1WI and T_2WI of tumor tissues

demonstrated the excellent T_1 effect and negative contrast effect of T_2WI at different time points (Figure 12G). In vivo results further revealed that the T_1WI and T_2WI in the tumor significantly changed at 2 h (∼0.4) and 4 h (∼0.28) post-injection of Fe_3O_4@HA, respectively (Figure 12E). Meanwhile, the $\Delta R_2/\Delta R_1$ ratio at the tumor site exhibited a marked increase at 8 h after the administration of Fe_3O_4@HA (Figure 12F). The T_1 imaging effect was largely weakened by the enhanced T_2 imaging of the Fe_3O_4@HA, so how to balance these two imaging-modes and obtain an optimized contrast effect should be carefully considered before their further application.

Activation. Among the tumor-specific stimuli, acidic pH and high GSH concentration in the tumor microenvironment have been widely used in responsive imaging.[122−126] Sun et al.[123] constructed a pH- and GSH-responsive $MnSiO_3$@Fe_3O_4 for dual-mode MRI. Under the condition of weak acidity and high GSH, the $MnSiO_3$@Fe_3O_4 dissociated, leading to the separation of IONPs and Mn^{2+}, and the recovery of dual-mode MRI imaging.

3.2. External Stimuli-Responsive Iron Oxide Nanoparticles for Tumor MR Imaging

External stimuli-responsive IONPs are another current area of increasing research focus with the advantages of controllability, non-invasiveness, and simple stimulation.[127] These formulations can be roughly divided based on the external stimuli: magnetic response, light response, and other response.

3.2.1. Magnetic-Responsive IONP-Based Contrast Agents. Due to their superparamagnetic properties, IONPs can be highly magnetized and thus target tumors under an applied magnetic field.[128,129] Targeting CAs with magnetic forces can be used to concentrate the MRI CAs at the target site, thus enhancing the imaging performance. Meanwhile, with the help of an external static magnetic field (SMF), significantly increased IONP uptake can be observed in
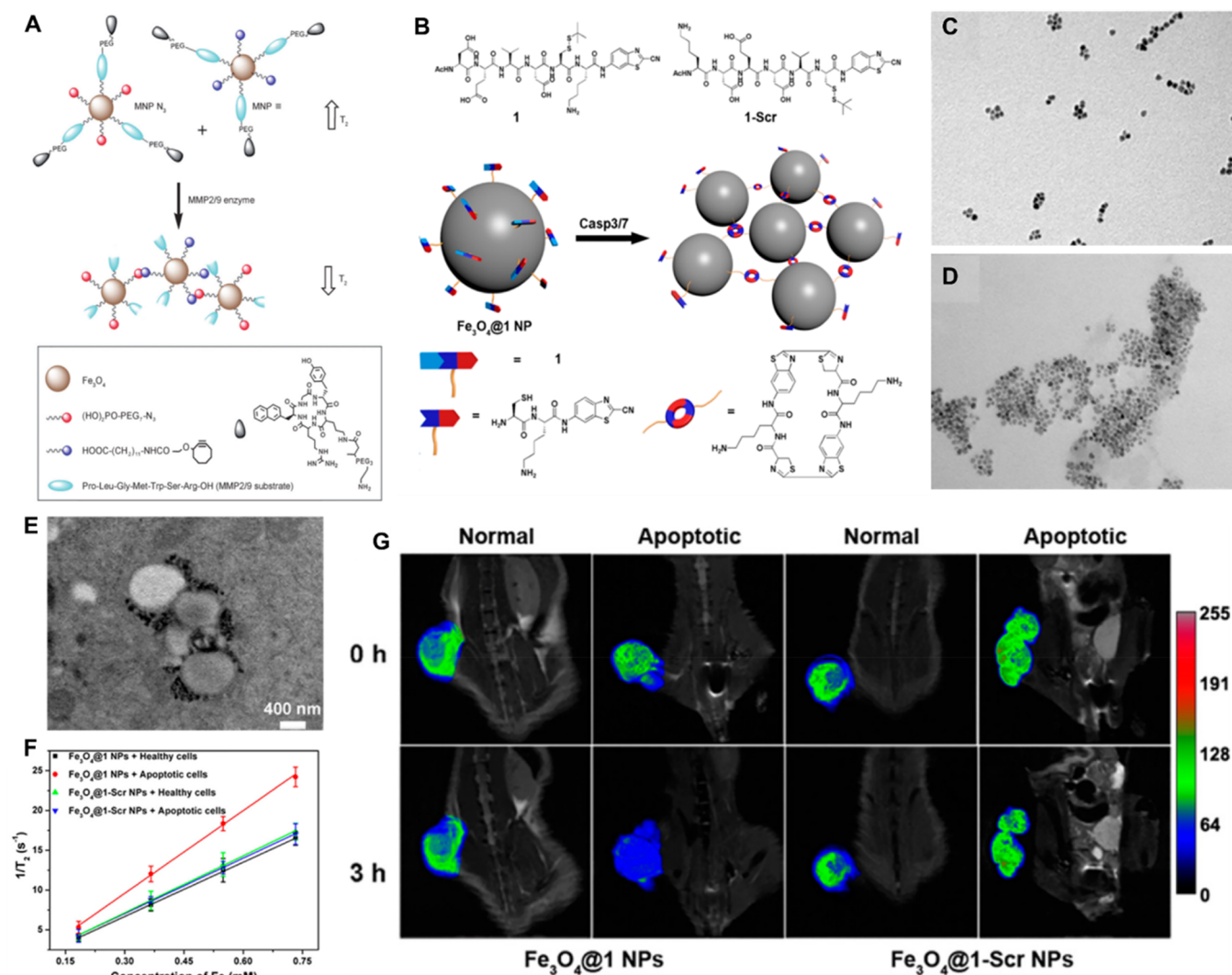
Figure 10. (A) Schematic illustration of in vitro and in vivo "clicking" NPs. Reprinted with permission from ref. 110. Copyright 2014 Wiley-VCH Verlag GmbH & Co. KGaA, Weinheim. (B) Chemical structures of **1** and **1**-Scr (scrambled control compound) and schematic illustration of intracellular Casp3/7-instructed aggregation of $Fe_3O_4@\mathbf{1}$ NPs. TEM images of (C) $Fe_3O_4@\mathbf{1}$ NPs and (D) $Fe_3O_4@\mathbf{1}$ NPs incubated with Casp3. (E) High-magnification TEM image of apoptotic HepG2 cells incubated with $Fe_3O_4@\mathbf{1}$ NPs. (F) $1/T_2$ of different NPs in the healthy and apoptotic cells. (G) In vivo coronal T_2WI of different groups at 0 or 3 h post-injection. Reprinted with permission from ref. 111. Copyright 2016 American Chemical Society.

tumor cells.[130−133] Bai et al.[131] developed triple-modal imaging magnetic nanocapsules that encapsulate hydrophobic SPIO NPs. When an SMF was applied to the tumor site for 1 h, the tumor uptake increased by about 3 times and about 2.2 times at 1 and 24 h, respectively. Moreover, Gu et al.[134] constructed a magnetic liposomal formulation loaded with SPIO NPs (Figure 13A). The application of external magnets promoted rapid internalization of tumor cells to SPIO NPs, evaluated by MRI (Figure 13B). However, the magnetization strength of each SPIO NP alone is relatively low. It is difficult to control their localization in relatively deeper organizations.

Several studies have used magnetic targeting combined with an active targeting strategy.[135−137] For example, Yang et al.[135] constructed adjustable magneto-vesicles (MVs) composed of densely arranged SPIO NPs (Figure 13C). MVs with a thicker membrane exhibited significant magnetic manipulation due to the large number of SPIO NPs in each vesicle. In addition, due to the synergistic effect of magnetic targeting and active targeting, MVs conjugated with targeted peptides can be

effectively accumulated in tumor sites (Figure 13D). The strength of the magnetic field strongly determines the imaging effect, which becomes the prerequisite to obtaining high-contrast images. However, high magnetic fields are not common in the lab, which limits the operability of experiments.

3.2.2. Light-Responsive IONP-Based Contrast Agents. Light-responsive nanoparticles are attractive options as externally activated CAs due to their spatiotemporal control properties.[138] Light can alter the surface modification of IONPs, thus changing their relaxation properties.

Disassembly. Louie and colleagues[139] combined a spyropyran derivative to IONPs. The light-induced changes in the conformity spyropyran between its hydrophobic and hydrophilic heterogeneity caused the nanoparticles' aggregation or dispersion (Figure 14A), shortening the T_2 relaxation time by $33.7 \pm 2.4\%$ under light irradiation (Figure 14B). Importantly, that work evaluated the relaxation effect of the synthesized IONPs, but did not include cell or in vivo experiments likely due to the limited penetration of UV light. Modifying the
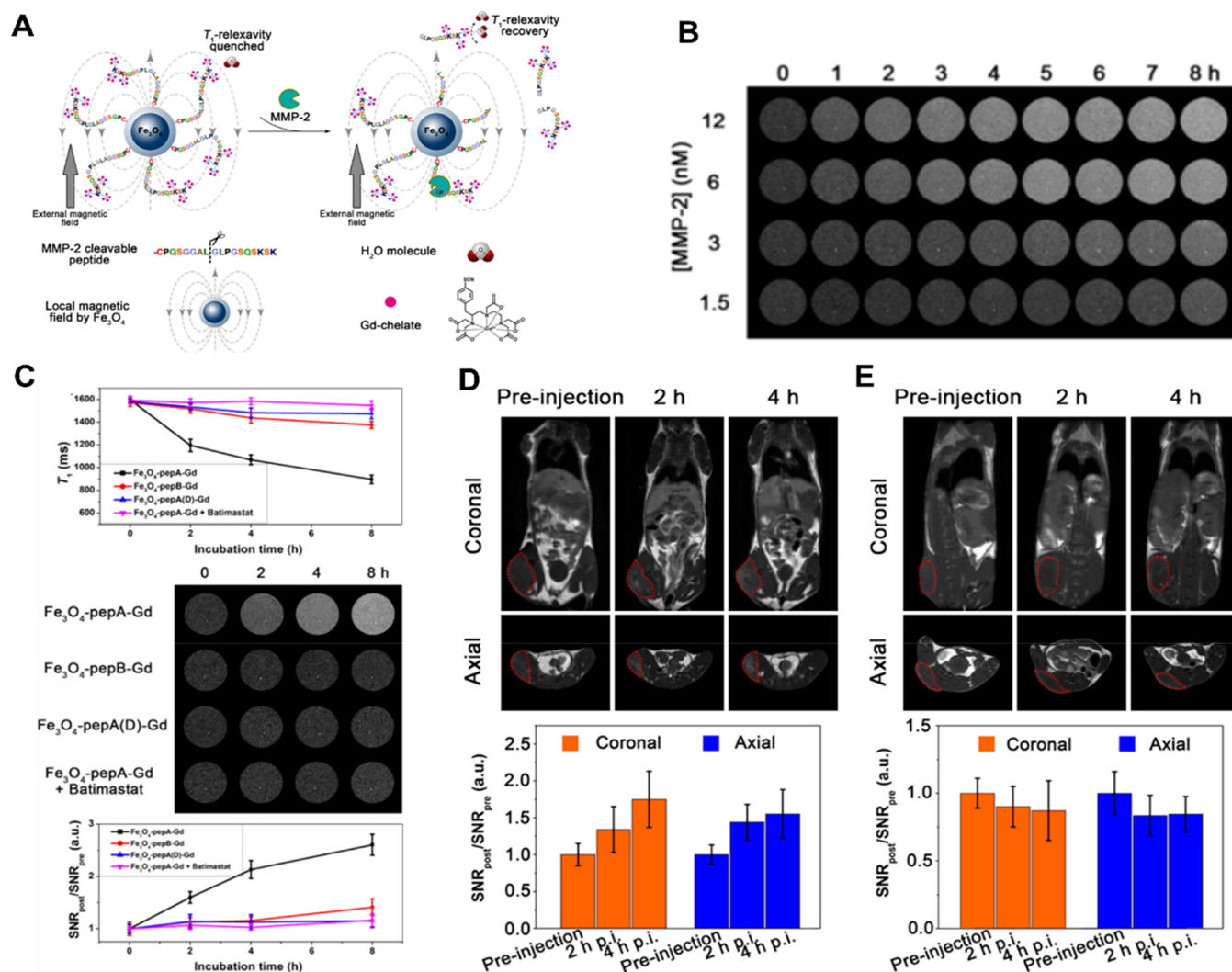
Figure 11. (A) Illustration of MMP-2 detection based on T_1 relaxivity recovery. (B) T_1WI of the IONP-based T_1 recovery system incubated with MMP-2. (C) T_1 measurements and T_1-weighted phantom imaging of Fe_3O_4−pepA−Gd, Fe_3O_4−pepB−Gd, and Fe_3O_4−pepA$_{(D)}$−Gd (uncleavable peptide for a negative control) conjugates. Fe_3O_4−pepA−Gd + Batimastat was the inhibition group. In vivo MMP sensing of the (D) responsive probe and (E) nonresponsive probe. Reprinted with permission from ref. 114. Copyright 2017 American Chemical Society.

surface of IONPs with a NIR light-responsive functional group may remedy this limitation in the future.

Assembly. Huang et al.[140] synthesized an Fe_3O_4 cluster-based, light-activated MRI probe (Ce_6/Fe_3O_4−M) by the encapsulation of Ce_6 into the core and the modification of the surface with an ROS-cleaved thioketal (TK) linker (Figure 15A). Under light irradiation, ROS triggered the degradation of the surface ligand and induced the aggregation of the Fe_3O_4 clusters (Figure 15D and E), thereby increasing the saturated magnetization (Figure 15B) and boosting the T_2 imaging signal (Figure 15C). The results of animal experiments further showed negatively enhanced T_2-weighted MR imaging of tumors during 3∼24 h after injection of the probe under NIR light irradiation (Figure 15F−H).

Few studies investigating light-responsive IONPs for tumor imaging have been reported; however, Shi et al.[141] reported light-addressable nanoclusters of USPIO NPs for inflammatory arthritis enhancement T_1/T_2-weighted MR imaging. We conjecture this stimuli-responsive imaging modality based on IONPs will be applied to tumor imaging in the future.

3.2.3. Other External Stimuli-Responsive IONP-Based Contrast Agents.

Although light and magnetic fields have attracted the greatest attention among external stimuli, other external stimuli-responsive IONPs have recently emerged, including heat and ultrasound. Laurent et al.[142] developed nanothermometers based on USPIOs with a thermosensitive polymer attached to the surface, which behave as positive CAs in low-field MRI. To achieve this, the authors grafted JeffamineM-2005, a commercial thermosensitive polymer, onto the surface of USPIOs using salinization and amide-bond coupling reactions. The nanothermometers exhibited temperature-responsive colloidal behavior, with their surface ligands reversibly altering to hydrophobic above a lower critical solution temperature (LCST; Figure 16A), resulting in a decreased USPIO r_1 value. Further applicability of this polymer-grafted USPIO will require improved stealth behavior of the polymer surface in order to efficiently prevent the gathering of the USPIOs in high-salinity buffers of plasma proteins, and maintain the temperature responsiveness of the coating. Ultrasound is also one of the common external stimuli.[143] Gu et al. prepared IONP-embedded microbubbles
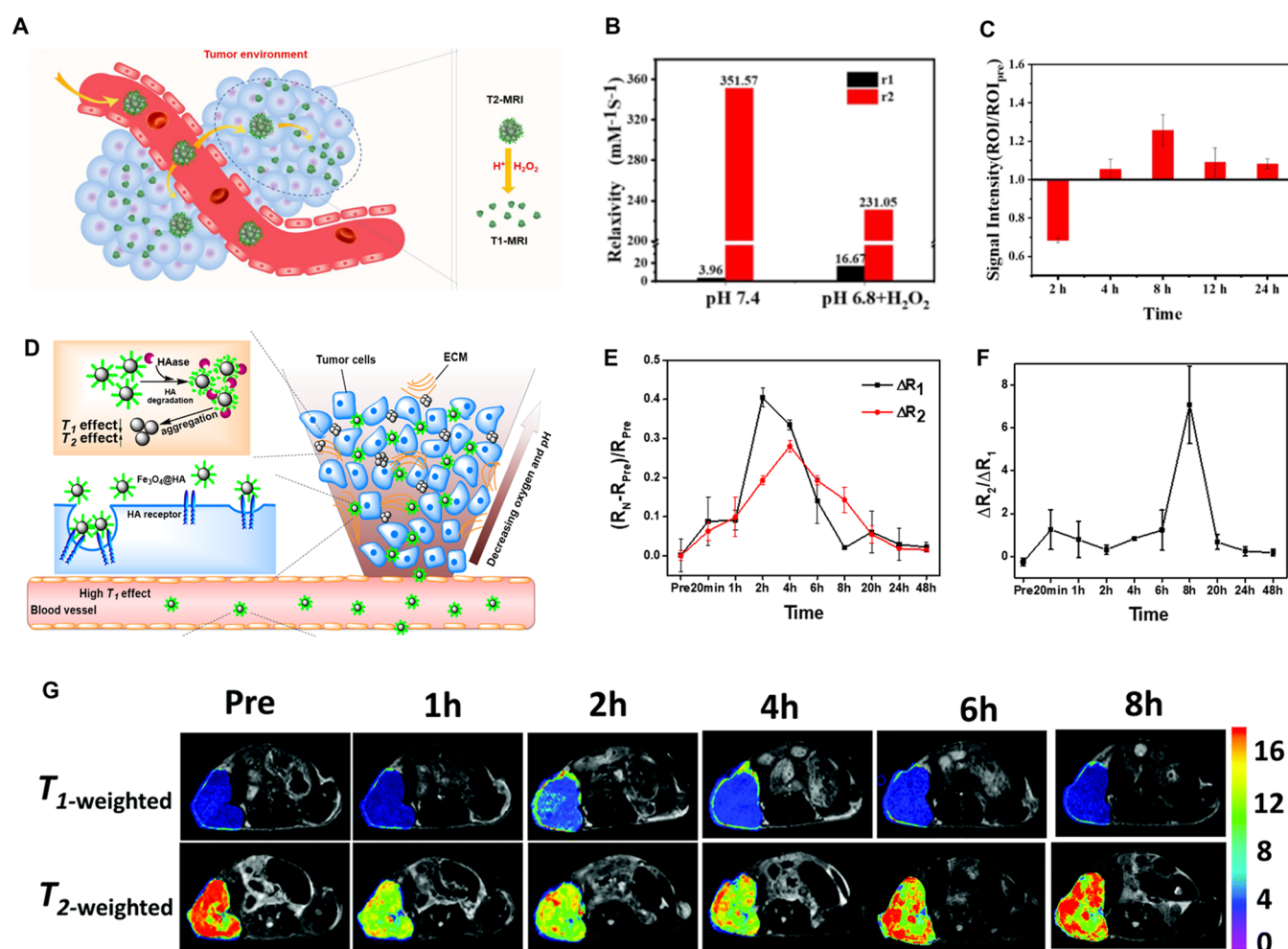
Figure 12. (A) Illustration of the sensing principle of USPIO nanoprobes. (B) Relaxivity data of USPIO nanoprobes in PBS (pH 7.4) and an acid buffer (pH 6.8) containing 100 μM H_2O_2. (C) Time-dependent T_1-weighted SNR of the tumor-bearing mice after injecting USPIONs@TA nanoprobes. Reprinted with permission from ref. 119. Copyright 2022 American Chemical Society. (D) Illustration of changes in MRI signals for the self-assembling Fe_3O_4@HA in a tumor site with abundant HAase and decreased pH. (E) Results from the analysis of T_1/T_2 maps. (F) $\Delta R_2/\Delta R_1$ ratio of the tumor site. (G) T_1 and T_2 mapping of nude mice bearing tumors before and after intravenous injection of Fe_3O_4@HA. Reprinted with permission from ref. 121. Copyright 2017 The Royal Society of Chemistry.

that exhibit controlled release of IONPs from shells into cells by ultrasonic excitation.[144] The authors observed that the IONPs embedded in the microbubble shells can enter tumor cells with control of the transmission rate by tuning the acoustic intensity (Figure 16B and C). Consequently, MRI can track the IONP-labeled cells noninvasively. However, balancing cell porosity and the integrity of the plasma membrane is important in the application of nanomaterials. This may be achieved by adjusting the acoustic intensity in future studies.

Multiple-responsive IONPs that are affected by both external and internal responses can be utilized for the targeted release of drugs at lesion sites and thus are applicable for specific tumor imaging.[145−151] Recently, Liu et al.[150] constructed a versatile nanoplatform based on IONPs with pH/thermal-response for improving cancer theranostics. With significant magnetic targeting effects, the nanoplatform was specifically accumulated in the tumor site to improve the imaging effect of MRI.

4. CONCLUSION AND PERSPECTIVES

Thanks to great strides in the development of IONPs preparation and surface modification technologies over the

last decades, the application of IONPs in tumor imaging has made considerable progress. Tumor single-mode and multi-mode imaging probes based on smart IONPs have now emerged.[152−154] In contrast to traditional MRI CAs with fixed contrast capacities, these stimuli-responsive MRI CAs can switch "on" or "off" T_1 and T_2 signal in response to specific stimuli in the lesion. Here, we have summarized the recent progress in constructing smart IONPs based on external and internal stimuli. Although countless studies have described numerous IONPs that can overcome the limitation of current MR imaging and improve diagnostic sensitivity, some challenges that limit their application in clinics still exist.

The magnetic properties of IONPs strongly affect their imaging signal in both T_1- and T_2-weighted modes.[31] Therefore, adjusting the chemical and physical properties of IONPs (such as crystallinity, structure, hydrophilicity, and so on) to control their behavior under different applied field strengths is a cornerstone of IONPs that may be applied in various areas. For example, a higher applied field strength can help us to collect clearer images.[155] However, the r_2 value of IONPs increases with field strength, which will significantly reduce the contrast of T_1WI. Reducing the crystallinity of
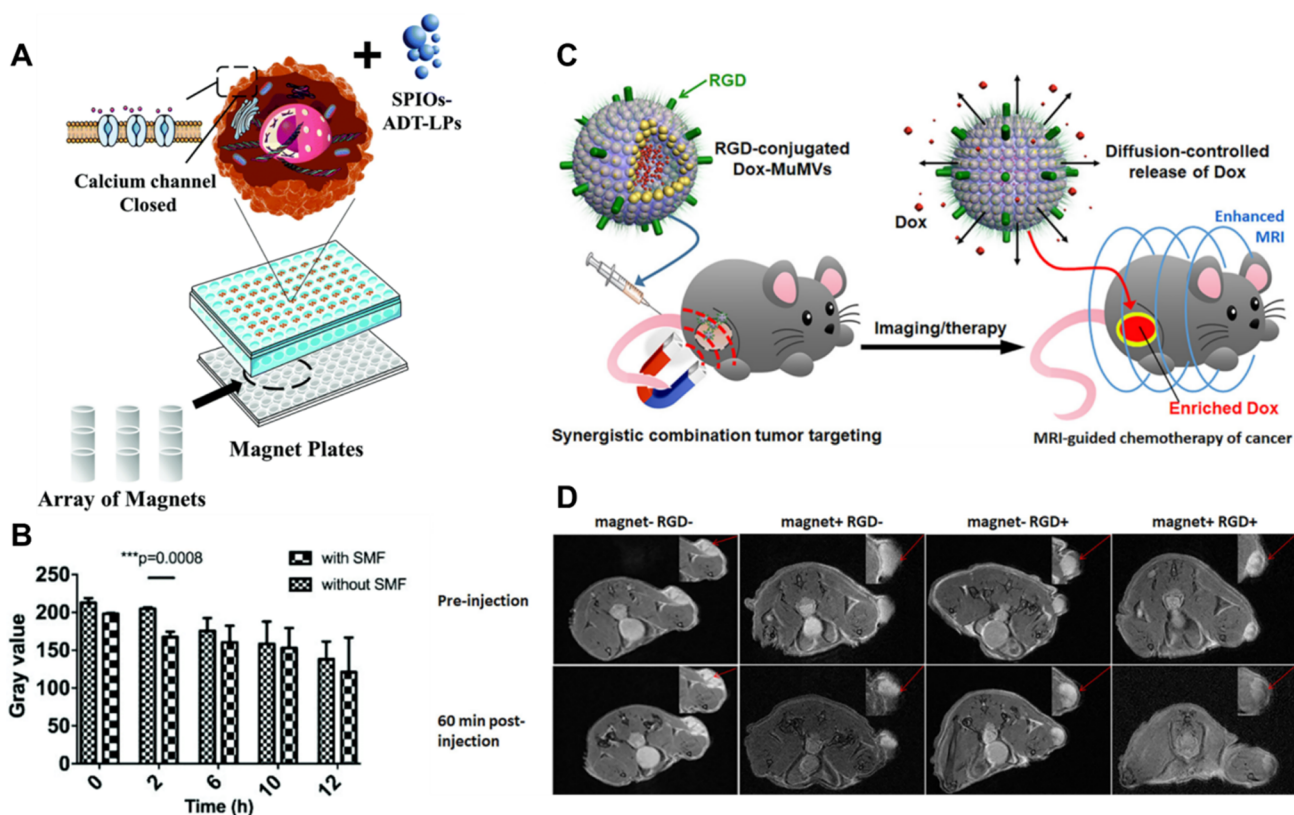
Figure 13. (A) Illustration of the magnetic liposomal formulation loaded with SPIO NPs. The magnet plates provided the magnetic force to spatially manipulate the nanoplatforms. (B) The gray intensities of T_2WI of the tumor cells after the indicated different times with the magnetic nanocapsules. Reprinted with permission from ref. 134. Copyright 2019 The Royal Society of Chemistry. (C) Illustration of the utilization of magneto-vesicles (MVs) for MRI-guided chemotherapy of tumors. (D) In vivo T_2WI of tumor areas (insets) 1 h after intravenous injection of the indicated treatments: MVs (magnet±) and RGD-MVs (magnet±). Reprinted with permission from ref. 135. Copyright 2018 American Chemical Society.
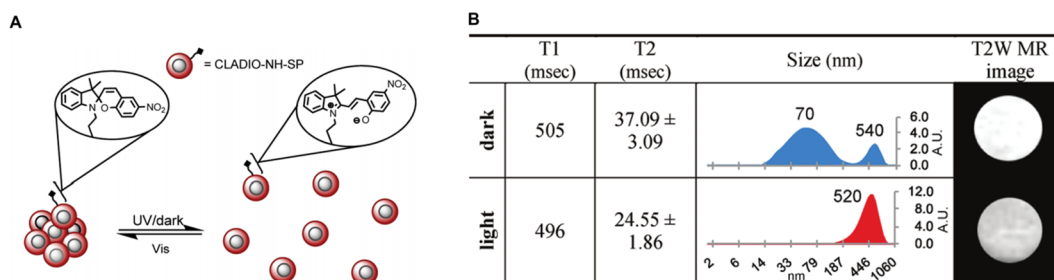
Figure 14. (A) Illustration of light-induced reversible agglomeration of IONPs coupled to a spyropyran derivative. (B) Relaxation time, size, and image data of NPs in the dark and with light stimulation. Reprinted with permission from ref. 139. Copyright 2010 American Chemical Society.

IONPs may be a method to improve the r_1/r_2 ratio to mitigate this effect.[25] However, this method is expected also to decrease the r_1 value, so a greater amount of CA would be required to be injected to obtain a similar effect, increasing the safety risk of the CA. Therefore, balancing the T_1 and T_2 signal is one of the major challenges to obtaining IONPs with excellent performance in different applications.

The fine construction of diverse surface ligands is a double-edged sword. Different surface modifications of IONPs may affect their blood compatibility and biological safety.[156,157] Meanwhile, the sensitivity of the responsive chemical bonds present on the surface of the nanoparticle, can greatly affect the effectiveness of the stimuli-responsive nanoplatform. The powerful designability of this strategy aids in selecting an appropriate method to achieve the desired CA behavior.

However, the numerous synthesis steps and complicated purification technologies described in the literature present a considerable obstacle for IONPs to achieve industrial-scale production and clinical application. Hence, simplifying the preparation method without reducing the response sensitivity should be another key factor to be considered in developing the next generation of smart IONP CAs. Further, evolving advanced synthetic technology can also significantly aid in closing the gap to realizing the large-scale production of IONPs with high utility.

Upon the injection of IONPs into the blood, IONPs tend to form an additional surface layer by interacting with biological matrices (such as plasma proteins and lipids), which largely defines the biological properties of IONPs and determines their fate within the body.[158−160] The MRI performance of
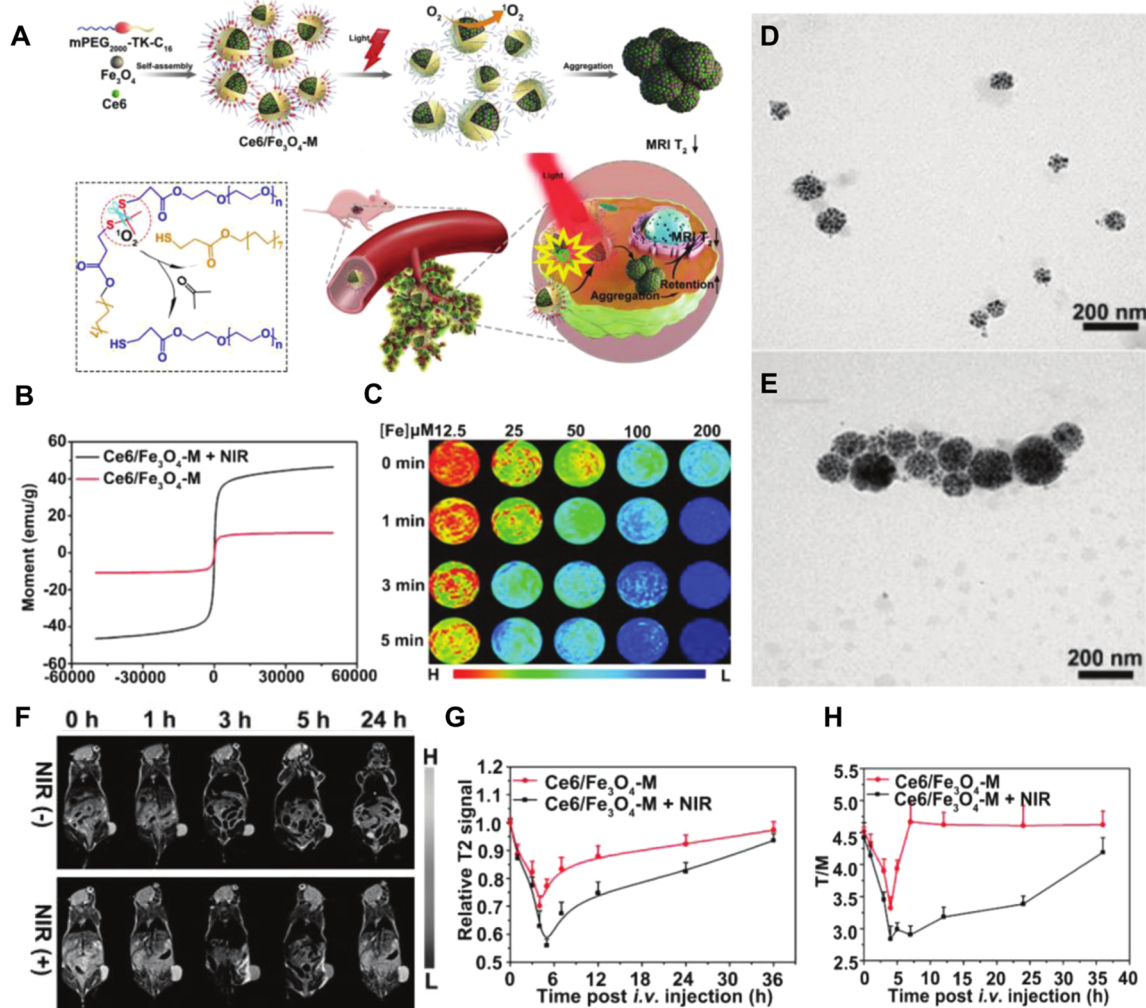
Figure 15. (A) Schematic illustration of the light-activated MRI probe (Ce_6/Fe_3O_4-M) and the mechanism of oxidation-triggered MRI enhancement generated by a laser. (B) Magnetization curve of Ce_6/Fe_3O_4-M before and after laser irradiation. (C) T_2-weighted pseudocolor images of Ce_6/Fe_3O_4-M for the different irradiation times. TEM images of Ce_6/Fe_3O_4-M (D) before and (E) after irradiation. (F) In vivo T_2-weighted pseudocolor images at the indicated times post-injection. One hour after intravenous injection of Ce_6/Fe_3O_4-M, using a 660 nm laser ($1.0~W \cdot cm^{-2}$) to irradiate the tumor for 10 min. (G) The relative T_2 signal intensity of tumors and (H) the T_2 ratio of the tumor to the muscle (T/M) without or with laser irradiation. Reprinted with permission from ref. 140. Copyright 2020 Wiley-VCH Verlag GmbH & Co. KGaA, Weinheim.
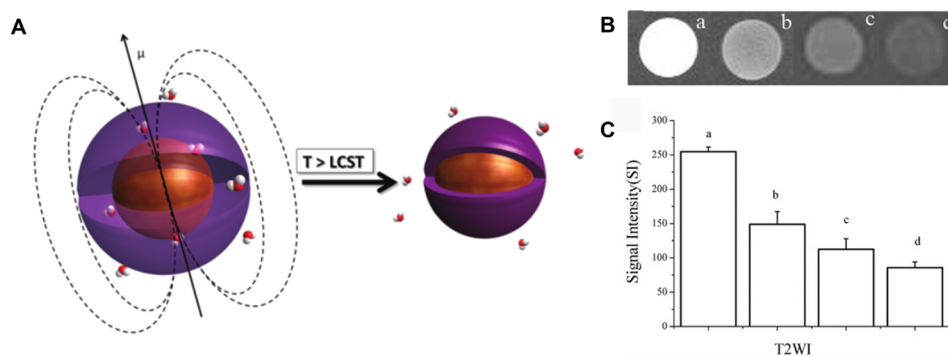
Figure 16. (A) Schematic illustration of the response of nanothermometers with thermosensitive polymer grafted ultrasmall IONPs. Reprinted with permission from ref. 142. Copyright 2015 The Royal Society of Chemistry. (B) T_2WI for cell solution: a) control, b) 0.1, c) 0.5, and d) 0.75 W cm^{-2} ultrasound and IONP-embedded microbubble treatments. (C) Bar graph showing the average signal intensity from the different samples on T_2WI. Reprinted with permission from ref. 144. Copyright 2011 Wiley-VCH Verlag GmbH & Co. KGaA, Weinheim.

IONPs strongly depends on the species and abundance of the adsorbed biological matrices.[161] Therefore, controlling the accumulation of biological molecules, such as proteins, on the surface of IONPs in the blood may help to avoid rapid clearance from the bloodstream, improving tumor target ability and retention time.[152] However, the key factors governing

protein adsorption remain unclear and require additional investigation. Fortunately, our research group has developed various strategies and methods to monitor the interactions between NPs and biological molecules, which will help us to understand the effects of nanoparticle parameters on the adsorption behavior.[162−164] For example, a fast and biolayer-interferometry-based fishing strategy was used to study how the physicochemical properties of NPs affect the protein adsorption process and the corresponding biological responses.[165] Additionally, Wang et al. evolved various synchrotron radiation analytical techniques to illustrate how coating ligands affect membrane integrity,[166] and to elucidate the valence of metal elements under various conditions.[167,168] In the future, these methods are expected to be used to study the interactions between biological molecules and IONPs, establishing the design principle for IONPs.

The human body contains the greatest amount of iron as an essential trace element. The metal participates in various biological processes, both physiological and pathophysiological.[168] However, excess iron deposition in the body will cause iron overload, which can lead to deleterious effects to organs or other complications.[169,170] In addition, large IONPs are metabolized to labile iron rather than excreted,[50] catalyzing hydroxyl radical production from ferrous iron, which can damage DNA, lipids, and proteins within cells.[171] Thus, sophisticated methods are urgently needed to reveal shifts in the valency of iron under various conditions and monitor the effect on the subsequent biological processes. Meanwhile, the long-term biological effects and metabolism of IONP CAs (especially in the liver) should be monitored after the collection of images.

With the continuous development of computing power in recent years, algorithms, and data, artificial intelligence (AI) techniques for medical image analysis have shown indexed growth, especially in tumor imaging.[172] Advancements in supercomputers, cloud computing platforms and the heterogeneous architecture of graphics processing unit (GPU) have significantly improved computing speed and reduced costs. The progress and iteration in image recognition algorithms and data processing algorithms for tumor characteristics can achieve excellent performance in image recognition and attains higher recognition accuracy.[173] With growing digital transformation in the medical field, the increasing availability of big data and the standardization of image acquisition have also promoted the prosperity of AI-based tools in healthcare, particularly in oncology image analysis.[174] The combination of AI and nanotechnology are just emerging, and reports about the nanoprobe, especially nanoprobe-based IONPs, are scarce. In the future, integrating AI data analysis techniques and the imaging cancer map of smart IONP nanoprobes may facilitate improving the detection sensitivity and realizing early screening of cancer.

The outstanding safety, regulable signal intensity, and biologically reusable properties of smart IONPs make them promising MRI CAs to reveal mechanisms at the biological molecular level, understand disease progression, detect the disease early, and monitor treatment efficacy. We hope this comprehensive review will inspire the future direction of the next-generation MRI CA based on IONP.

■ AUTHOR INFORMATION

Corresponding Authors

Chunying Chen − *CAS Key Laboratory for Biomedical Effects of Nanoparticles and Nanosafety & CAS Center for Excellence in Nanoscience, National Center for Nanoscience and Technology, Beijing 100190, China; University of Chinese Academy of Sciences, Beijing 100049, China; Research Unit of Nanoscience and Technology, Chinese Academy of Medical Sciences, Beijing 100021, China; The GBA National Institute for Nanotechnology Innovation, Guangzhou 510700, China;* ⓘ orcid.org/0000-0002-6027-0315; Email: chenchy@nanoctr.cn

Junfang Xian − *Department of Radiology, Beijing Tongren Hospital, Capital Medical University, Beijing 100730, China;* Email: cjr.xianjunfang@vip.163.com

Huige Zhou − *CAS Key Laboratory for Biomedical Effects of Nanoparticles and Nanosafety & CAS Center for Excellence in Nanoscience, National Center for Nanoscience and Technology, Beijing 100190, China; University of Chinese Academy of Sciences, Beijing 100049, China; Research Unit of Nanoscience and Technology, Chinese Academy of Medical Sciences, Beijing 100021, China;* ⓘ orcid.org/0000-0001-6210-0566; Email: zhouhg@nanoctr.cn

Authors

Zhenzhen Li − *CAS Key Laboratory for Biomedical Effects of Nanoparticles and Nanosafety & CAS Center for Excellence in Nanoscience, National Center for Nanoscience and Technology, Beijing 100190, China; Department of Radiology, Beijing Tongren Hospital, Capital Medical University, Beijing 100730, China*

Ru Bai − *CAS Key Laboratory for Biomedical Effects of Nanoparticles and Nanosafety & CAS Center for Excellence in Nanoscience, National Center for Nanoscience and Technology, Beijing 100190, China; University of Chinese Academy of Sciences, Beijing 100049, China; Research Unit of Nanoscience and Technology, Chinese Academy of Medical Sciences, Beijing 100021, China*

Jia Yi − *Guangdong Provincial Development and Reform Commission, Guangzhou 510031, China*

Complete contact information is available at:
https://pubs.acs.org/10.1021/cbmi.3c00026

Notes

The authors declare no competing financial interest.

■ GLOSSARY

1. IONP-based contrast agents:Contrast agents containing iron oxide nanoparticles as the major component.

2. Smart IONPs:Iron oxide nanoparticles with regulated signal intensity under different conditions.

3. Iron oxide aggregations:Particles of relatively large size, occurring when single iron oxide nanoparticles aggregate under certain stimuli, such as pH, enzyme, etc.

4. Dual-mode MRI CAs:MR imaging contrast agents that integrate T_1- and T_2-weighted MR imaging.

5. Activating images signal:Image signals of two- or multitype contrast agents only recovered when separated via specific stimuli, selectively improving the lesion's contrast.

■ REFERENCES

(1) Bruno, F.; Arrigoni, F.; Mariani, S.; Splendiani, A.; Di Cesare, E.; Masciocchi, C.; Barile, A. Advanced magnetic resonance imaging (MRI) of soft tissue tumors: techniques and applications. *Radiol Med.* **2019**, *124*, 243.

(2) Cai, H.; Dai, X.; Wang, X.; Tan, P.; Gu, L.; Luo, Q.; Zheng, X.; Li, Z.; Zhu, H.; Zhang, H.; Gu, Z.; Gong, Q.; Luo, K. A nanostrategy for efficient imaging-guided antitumor therapy through a stimuli-responsive branched polymeric prodrug. *Adv. Sci.* **2020**, *7*, 1903243.

(3) Yang, L. M.; Zheng, H.; Ratnakar, J. S.; Adebesin, B. Y.; Do, Q. N.; Kovacs, Z.; Blount, P. Engineering a pH-sensitive liposomal MRI agent by modification of a bacterial channel. *Small* **2018**, *14*, e1704256.

(4) Thu, M. S.; Bryant, L. H.; Coppola, T.; Jordan, E. K.; Budde, M. D.; Lewis, B. K.; Chaudhry, A.; Ren, J.; Varma, N. R.; Arbab, A. S.; Frank, J. A. Self-assembling nanocomplexes by combining ferumoxytol, heparin and protamine for cell tracking by magnetic resonance imaging. *Nat. Med.* **2012**, *18*, 463.

(5) Jeon, M.; Halbert, M. V.; Stephen, Z. R.; Zhang, M. Iron oxide nanoparticles as T1 contrast agents for magnetic resonance imaging: fundamentals, challenges, applications, and prospectives. *Adv. Mater.* **2021**, *33*, e1906539.

(6) Fu, S.; Cai, Z.; Ai, H. Stimulus-responsive nanoparticle magnetic resonance imaging contrast agents: design considerations and applications. *Adv. Healthc Mater.* **2021**, *10*, e2001091.

(7) Shin, T. H.; Choi, Y.; Kim, S.; Cheon, J. Recent advances in magnetic nanoparticle-based multi-modal imaging. *Chem. Soc. Rev.* **2015**, *44*, 4501.

(8) Clough, T. J.; Jiang, L.; Wong, K. L.; Long, N. J. Ligand design strategies to increase stability of gadolinium-based magnetic resonance imaging contrast agents. *Nat. Commun.* **2019**, *10*, 1420.

(9) Ni, D.; Bu, W.; Ehlerding, E. B.; Cai, W.; Shi, J. Engineering of inorganic nanoparticles as magnetic resonance imaging contrast agents. *Chem. Soc. Rev.* **2017**, *46*, 7438.

(10) Tong, S.; Hou, S.; Zheng, Z.; Zhou, J.; Bao, G. Coating optimization of superparamagnetic iron oxide nanoparticles for high T2 relaxivity. *Nano Lett.* **2010**, *10*, 4607.

(11) Caravan, P.; Ellison, J. J.; McMurry, T. J.; Lauffer, R. B. Gadolinium(III) chelates as MRI contrast agents: structure, dynamics, and applications. *Chem. Rev.* **1999**, *99*, 2293.

(12) Werner, E. J.; Datta, A.; Jocher, C. J.; Raymond, K. N. High-relaxivity MRI contrast agents: where coordination chemistry meets medical imaging. *Angew. Chem., Int. Ed. Engl.* **2008**, *47*, 8568.

(13) Peng, Y. K.; Tsang, S.; Chou, P. T. Chemical design of nanoprobes for T1-weighted magnetic resonance imaging. *Mater. Today* **2016**, *19*, 336.

(14) Lu, Y.; Xu, Y.-J.; Zhang, G.-b.; Ling, D.; Wang, M.-q.; Zhou, Y.; Wu, Y.-D.; Wu, T.; Hackett, M. J.; Hyo Kim, B.; Chang, H.; Kim, J.; Hu, X.-T.; Dong, L.; Lee, N.; Li, F.; He, J.-C.; Zhang, L.; Wen, H.-Q.; Yang, B.; Hong Choi, S.; Hyeon, T.; Zou, D.-H. Iron oxide nanoclusters for T (1) magnetic resonance imaging of non-human primates. *Nat. Biomed. Eng.* **2017**, *1*, 637.

(15) Kabalka, G. W.; Davis, M. A.; Holmberg, E.; Maruyama, K.; Huang, L. Gadolinium-labeled liposomes containing amphiphilic Gd-DTPA derivatives of varying chain length: targeted MRI contrast enhancement agents for the liver. *Magn Reson Imaging* **1991**, *9*, 373.

(16) Kabalka, G. W.; Davis, M. A.; Moss, T. H.; Buonocore, E.; Hubner, K.; Holmberg, E.; Maruyama, K.; Huang, L. Gadolinium-labeled liposomes containing various amphiphilic Gd-DTPA derivatives: targeted MRI contrast enhancement agents for the liver. *Magn Reson Med.* **1991**, *19*, 406.

(17) Sherry, A. D.; Cacheris, W. P.; Kuan, K. T. Stability constants for Gd3+ binding to model DTPA-conjugates and DTPA-proteins: implications for their use as magnetic resonance contrast agents. *Magn Reson Med.* **1988**, *8*, 180.

(18) Hermann, P.; Kotek, J.; Kubícek, V.; Lukes, I. Gadolinium(III) complexes as MRI contrast agents: ligand design and properties of the complexes. *Dalton Trans* **2008**, *23*, 3027.

(19) Rogosnitzky, M.; Branch, S. Gadolinium-based contrast agent toxicity: a review of known and proposed mechanisms. *Biometals* **2016**, *29*, 365.

(20) Kuo, P. H.; Kanal, E.; Abu-Alfa, A. K.; Cowper, S. E. Gadolinium-based MR contrast agents and nephrogenic systemic fibrosis. *Radiology* **2007**, *242*, 647.

(21) Todd, D. J.; Kay, J. Gadolinium-induced fibrosis. *Annu. Rev. Med.* **2016**, *67*, 273.

(22) Hasebroock, K. M.; Serkova, N. J. Toxicity of MRI and CT contrast agents. *Expert Opin Drug Metab Toxicol* **2009**, *5*, 403.

(23) Lee, N.; Yoo, D.; Ling, D.; Cho, M. H.; Hyeon, T.; Cheon, J. Iron oxide based nanoparticles for multimodal imaging and magnetoresponsive therapy. *Chem. Rev.* **2015**, *115*, 10637.

(24) Zhao, Z.; Li, M.; Zeng, J.; Huo, L.; Liu, K.; Wei, R.; Ni, K.; Gao, J. Recent advances in engineering iron oxide nanoparticles for effective magnetic resonance imaging. *Bioact Mater.* **2022**, *12*, 214.

(25) Ling, D.; Lee, N.; Hyeon, T. Chemical synthesis and assembly of uniformly sized iron oxide nanoparticles for medical applications. *Acc. Chem. Res.* **2015**, *48*, 1276.

(26) Tong, S.; Hou, S.; Zheng, Z.; Zhou, J.; Bao, G. Coating optimization of superparamagnetic iron oxide nanoparticles for high T2 relaxivity. *Nano Lett.* **2010**, *10*, 4607.

(27) Arbab, A. S.; Yocum, G. T.; Kalish, H.; Jordan, E. K.; Anderson, S. A.; Khakoo, A. Y.; Read, E. J.; Frank, J. A. Efficient magnetic cell labeling with protamine sulfate complexed to ferumoxides for cellular MRI. *Blood* **2004**, *104*, 1217.

(28) Mori, K.; Fukuda, K.; Asaoka, H.; Ueda, T.; Kunimatsu, A.; Okamoto, Y.; Nasu, K.; Fukunaga, K.; Morishita, Y.; Minami, M. Radiofrequency ablation of the liver: determination of ablative margin at MR imaging with impaired clearance of ferucarbotran–feasibility study. *Radiology* **2009**, *251*, 557.

(29) Shen, Z.; Wu, A.; Chen, X. Iron oxide nanoparticle based contrast agents for magnetic resonance imaging. *Mol. Pharmaceutics* **2017**, *14*, 1352.

(30) Deng, L. H.; Jiang, H.; Lu, F. L.; Wang, H. W.; Pu, Y.; Wu, C. Q.; Tang, H. J.; Xu, Y.; Chen, T. W.; Zhu, J.; Shen, C. Y.; Zhang, X. M. Size and PEG length-controlled PEGylated monocrystalline superparamagnetic iron oxide nanocomposite for MRI contrast agent. *Int. J. Nanomedicine* **2021**, *16*, 201.

(31) Lee, N.; Hyeon, T. Designed synthesis of uniformly sized iron oxide nanoparticles for efficient magnetic resonance imaging contrast agents. *Chem. Soc. Rev.* **2012**, *41*, 2575.

(32) Kang, T.; Li, F.; Baik, S.; Shao, W.; Ling, D.; Hyeon, T. Surface design of magnetic nanoparticles for stimuli-responsive cancer imaging and therapy. *Biomaterials* **2017**, *136*, 98.

(33) Zhou, Z.; Yang, L.; Gao, J.; Chen, X. Structure-relaxivity relationships of magnetic nanoparticles for magnetic resonance imaging. *Adv. Mater.* **2019**, *31*, e1804567.

(34) Park, J. H.; von Maltzahn, G.; Zhang, L.; Schwartz, M. P.; Ruoslahti, E.; Bhatia, S. N.; Sailor, M. J. Magnetic iron oxide nanoworms for tumor targeting and imaging. *Adv. Mater.* **2008**, *20*, 1630.

(35) Jia, Z.; Song, L.; Zang, F.; Song, J.; Zhang, W.; Yan, C.; Xie, J.; Ma, Z.; Ma, M.; Teng, G.; Gu, N.; Zhang, Y. Active-target T1-weighted MR imaging of tiny hepatic tumor via RGD modified ultrasmall Fe3O4 nanoprobes. *Theranostics* **2016**, *6*, 1780.

(36) Landmark, K. J.; DiMaggio, S.; Ward, J.; Kelly, C.; Vogt, S.; Hong, S.; Kotlyar, A.; Myc, A.; Thomas, T. P.; Penner-Hahn, J. E.; Baker, J. R.; Holl, M. M. B.; Orr, B. G. Synthesis, characterization, and in vitro testing of superparamagnetic iron oxide nanoparticles targeted using folic acid-conjugated dendrimers. *ACS Nano* **2008**, *2*, 773.

(37) Li, C.; Chen, T.; Ocsoy, I.; Zhu, G.; Yasun, E.; You, M.; Wu, C.; Zheng, J.; Song, E.; Huang, C. Z.; Tan, W. Gold-coated Fe(3)O(4) nanoroses with five unique functions for cancer cell targeting, imaging and therapy. *Adv. Funct. Mater.* **2014**, *24*, 1772.

(38) Hauser, A. K.; Mitov, M. I.; Daley, E. F.; McGarry, R. C.; Anderson, K. W.; Hilt, J. Z. Targeted iron oxide nanoparticles for the enhancement of radiation therapy. *Biomaterials* **2016**, *105*, 127.

(39) Xu, Y.; Baiu, D. C.; Sherwood, J. A.; Mcelreath, M. R.; Qin, Y.; Lackey, K. H.; Otto, M.; Bao, Y. Linker-free conjugation and specific cell targeting of antibody functionalized iron-oxide nanoparticles. *J. Mater. Chem. B* **2014**, *2*, 6198.

(40) Luo, Y.; Yang, J.; Yan, Y.; Li, J.; Shen, M.; Zhang, G.; Mignani, S.; Shi, X. RGD-functionalized ultrasmall iron oxide nanoparticles for targeted T(1)-weighted MR imaging of gliomas. *Nanoscale* **2015**, *7*, 14538.

(41) Zhao, S.; Yu, X.; Qian, Y.; Chen, W.; Shen, J. Multifunctional magnetic iron oxide nanoparticles: an advanced platform for cancer theranostics. *Theranostics* **2020**, *10*, 6278.

(42) Wang, A.; Han, X.; Qi, W.; Du, S.; Jiang, Z.; Tang, X. The design of abnormal microenvironment responsive MRI nanoprobe and its application. *Int. J. Mol. Sci.* **2021**, *22*, 5147.

(43) Low, L. E.; Lim, H. P.; Ong, Y. S.; Siva, S. P.; Sia, C. S.; Goh, B. H.; Chan, E. S.; Tey, B. T. Stimuli-controllable iron oxide nanoparticle assemblies: design, manipulation and bio-applications. *J. Controlled Release* **2022**, *345*, 231.

(44) Cai, Z.; Wu, C.; Yang, L.; Wang, D.; Ai, H. Assembly-controlled magnetic nanoparticle clusters as MRI contrast agents. *ACS Biomater Sci. Eng.* **2020**, *6*, 2533.

(45) Ellis, C. M.; Pellico, J.; Davis, J. J. Magnetic nanoparticles supporting bio-responsive T1/T2 magnetic resonance imaging. *Materials* **2019**, *12*, 4096.

(46) Chen, R.; Ling, D.; Zhao, L.; Wang, S.; Liu, Y.; Bai, R.; Baik, S.; Zhao, Y.; Chen, C.; Hyeon, T. Parallel comparative studies on mouse toxicity of oxide nanoparticle- and gadolinium-based T1MRI contrast agents. *ACS Nano* **2015**, *9*, 12425.

(47) Weng, Q.; Hu, X.; Zheng, J.; Xia, F.; Wang, N.; Liao, H.; Liu, Y.; Kim, D.; Liu, J.; Li, F.; He, Q.; Yang, B.; Chen, C.; Hyeon, T.; Ling, D. Toxicological risk assessments of iron oxide nanocluster- and gadolinium-based T1MRI contrast agents in renal failure rats. *ACS Nano* **2019**, *13*, 6801.

(48) Reddy, L. H.; Arias, J. L.; Nicolas, J.; Couvreur, P. Magnetic nanoparticles: design and characterization, toxicity and biocompatibility, pharmaceutical and biomedical applications. *Chem. Rev.* **2012**, *112*, 5818.

(49) Zhao, Z.; Zhou, Z.; Bao, J.; Wang, Z.; Hu, J.; Chi, X.; Ni, K.; Wang, R.; Chen, X.; Chen, Z.; Gao, J. Octapod iron oxide nanoparticles as high-performance T2 contrast agents for magnetic resonance imaging. *Nat. Commun.* **2013**, *4*, 2266.

(50) Wahsner, J.; Gale, E. M.; Rodríguez-Rodríguez, A.; Caravan, P. Chemistry of MRI contrast agents: current challenges and new frontiers. *Chem. Rev.* **2019**, *119*, 957.

(51) Chouly, C.; Pouliquen, D.; Lucet, I.; Jeune, J. J.; Jallet, P. Development of superparamagnetic nanoparticles for MRI: effect of particle size, charge and surface nature on biodistribution. *J. Microencapsul* **1996**, *13*, 245.

(52) Soo Choi, H.; Liu, W.; Misra, P.; Tanaka, E.; Zimmer, J. P; Itty Ipe, B.; Bawendi, M. G; Frangioni, J. V Renal clearance of quantum dots. *Nat. Biotechnol.* **2007**, *25*, 1165.

(53) Reimer, P.; Müller, M.; Marx, C.; Wiedermann, D.; Muller, R.; Rummeny, E. J.; Ebert, W.; Shamsi, K.; Peters, P. E. T1 effects of a bolus-injectable superparamagnetic iron oxide, SH U 555 A: dependence on field strength and plasma concentration–preliminary clinical experience with dynamic T1-weighted MR imaging. *Radiology* **1998**, *209*, 831.

(54) Reimer, P.; Balzer, T. Ferucarbotran (Resovist): a new clinically approved RES-specific contrast agent for contrast-enhanced MRI of the liver: properties, clinical development, and applications. *Eur. Radiol* **2003**, *13*, 1266.

(55) Wood, M. L.; Hardy, P. A. Proton relaxation enhancement. *J. Magn Reson Imaging* **1993**, *3*, 149.

(56) Peng, Y. K.; Tsang, S.; Chou, P. T. Chemical design of nanoprobes for T1-weighted magnetic resonance imaging. *Mater. Today* **2016**, *19*, 336.

(57) Miao, Y.; Zhang, H.; Cai, J.; Chen, Y.; Ma, H.; Zhang, S.; Yi, J. B.; Liu, X.; Bay, B. H.; Guo, Y.; Zhou, X.; Gu, N.; Fan, H. Structure-relaxivity mechanism of an ultrasmall ferrite nanoparticle T(1) MR contrast agent: the impact of dopants controlled crystalline core and surface disordered shell. *Nano Lett.* **2021**, *21*, 1115.

(58) Zhou, Z.; Zhao, Z.; Zhang, H.; Wang, Z.; Chen, X.; Wang, R.; Chen, Z.; Gao, J. Interplay between longitudinal and transverse contrasts in Fe3O4 nanoplates with (111) exposed surfaces. *ACS Nano* **2014**, *8*, 7976.

(59) Villaraza, A. J.; Bumb, A.; Brechbiel, M. W. Macromolecules, dendrimers, and nanomaterials in magnetic resonance imaging: the interplay between size, function, and pharmacokinetics. *Chem. Rev.* **2010**, *110*, 2921.

(60) Zheng, X. Y.; Zhao, K.; Tang, J.; Wang, X. Y.; Li, L. D.; Chen, N. X.; Wang, Y. J.; Shi, S.; Zhang, X.; Malaisamy, S.; Sun, L. D.; Wang, X.; Chen, C.; Yan, C. H. Gd-dots with strong ligand-water interaction for ultrasensitive magnetic resonance renography. *ACS Nano* **2017**, *11*, 3642.

(61) Xu, S.; Wang, J.; Wei, Y.; Zhao, H.; Tao, T.; Wang, H.; Wang, Z.; Du, J.; Wang, H.; Qian, J.; Ma, K.; Wang, J. In situ one-pot synthesis of Fe(2)O(3)@BSA core-shell nanoparticles as enhanced T(1)-weighted magnetic resonance imaging contrast agents. *ACS Appl. Mater. Interfaces* **2020**, *12*, 56701.

(62) Aryal, S.; Key, J.; Stigliano, C.; Ananta, J. S.; Zhong, M.; Decuzzi, P. Engineered magnetic hybrid nanoparticles with enhanced relaxivity for tumor imaging. *Biomaterials* **2013**, *34*, 7725.

(63) Andrade, R.; Veloso, S.; Castanheira, E. Shape anisotropic iron oxide-based magnetic nanoparticles: synthesis and biomedical applications. *Int. J. Mol. Sci.* **2020**, *21*, 2455.

(64) Ai, H.; Flask, C.; Weinberg, B.; Shuai, X.; Pagel, M. D.; Farrell, D.; Duerk, J.; Gao, J. Magnetite-loaded polymeric micelles as ultrasensitive magnetic-resonance probes. *Adv. Mater.* **2005**, *17*, 1949.

(65) Chen, F.; Ward, J.; Robinson, P. J. MR imaging of the liver and spleen: a comparison of the effects on signal intensity of two superparamagnetic iron oxide agents. *Magn Reson Imaging* **1999**, *17*, 549.

(66) Choi, J. Y.; Kim, M. J.; Kim, J. H.; Kim, S. H.; Ko, H. K.; Lim, J. S.; Oh, Y. T.; Chung, J. J.; Yoo, H. S.; Lee, J. T.; Kim, K. W. Detection of hepatic metastasis: manganese- and ferucarbotran-enhanced MR imaging. *Eur. J. Radiol* **2006**, *60*, 84.

(67) Wang, Y. X.; Hussain, S. M.; Krestin, G. P. Superparamagnetic iron oxide contrast agents: physicochemical characteristics and applications in MR imaging. *Eur. Radiol* **2001**, *11*, 2319.

(68) Neuwelt, A.; Sidhu, N.; Hu, C. A.; Mlady, G.; Eberhardt, S. C.; Sillerud, L. O. Iron-based superparamagnetic nanoparticle contrast agents for MRI of infection and inflammation. *AJR Am. J. Roentgenol* **2015**, *204*, W302.

(69) Huang, Y.; Hsu, J. C.; Koo, H.; Cormode, D. P. Repurposing ferumoxytol: diagnostic and therapeutic applications of an FDA-approved nanoparticle. *Theranostics* **2022**, *12*, 796.

(70) Cao, Y.; He, Y.; Mao, Z.; Kuang, Y.; Liu, M.; Zhang, Y.; Pei, R. Synergistic regulation of longitudinal and transverse relaxivity of extremely small iron oxide nanoparticles (ESIONPs) using pH-responsive nanoassemblies. *Nanoscale* **2020**, *12*, 17502.

(71) Liu, W.; Yin, S.; Hu, Y.; Deng, T.; Li, J. Microemulsion-confined biomineralization of PEGylated ultrasmall Fe3O4 nano-

crystals for T2-T1 switchable MRI of tumors. *Anal. Chem.* **2021**, *93*, 14223.

(72) Ling, D.; Park, W.; Park, S. J.; Lu, Y.; Kim, K. S.; Hackett, M. J.; Kim, B. H.; Yim, H.; Jeon, Y. S.; Na, K.; Hyeon, T. Multifunctional tumor pH-sensitive self-assembled nanoparticles for bimodal imaging and treatment of resistant heterogeneous tumors. *J. Am. Chem. Soc.* **2014**, *136*, 5647.

(73) Hou, J.; Liu, H.; Ma, Q.; Xu, S.; Wang, L. Coordination-driven self-assembly of iron oxide nanoparticles for tumor microenvironment-responsive magnetic resonance imaging. *Anal. Chem.* **2022**, *94*, 15578.

(74) Li, F.; Liang, Z.; Liu, J.; Sun, J.; Hu, X.; Zhao, M.; Liu, J.; Bai, R.; Kim, D.; Sun, X.; Hyeon, T.; Ling, D. Dynamically reversible iron oxide nanoparticle assemblies for targeted amplification of T1-weighted magnetic resonance imaging of tumors. *Nano Lett.* **2019**, *19*, 4213.

(75) Lu, J.; Sun, J.; Li, F.; Wang, J.; Liu, J.; Kim, D.; Fan, C.; Hyeon, T.; Ling, D. Highly sensitive diagnosis of small hepatocellular carcinoma using pH-responsive iron oxide nanocluster assemblies. *J. Am. Chem. Soc.* **2018**, *140*, 10071.

(76) He, Y.; Mao, Z.; Zhang, Y.; Lv, H.; Yan, J.; Cao, Y.; Pei, R. Tumor acid microenvironment-triggered self-assembly of ESIONPs for T1 /T2 switchable magnetic resonance imaging. *ACS Appl. Bio Mater.* **2020**, *3*, 7752.

(77) Zhang, X.; Lu, H.; Tang, N.; Chen, A.; Wei, Z.; Cao, R.; Zhu, Y.; Lin, L.; Li, Q.; Wang, Z.; Tian, L. Low-power magnetic resonance-guided focused ultrasound tumor ablation upon controlled accumulation of magnetic nanoparticles by cascade-activated DNA cross-linkers. *ACS Appl. Mater. Interfaces* **2022**, *14*, 31677.

(78) Yang, H. Y.; Jang, M. S.; Li, Y.; Fu, Y.; Wu, T. P.; Lee, J. H.; Lee, D. S. Hierarchical tumor acidity-responsive self-assembled magnetic nanotheranostics for bimodal bioimaging and photodynamic therapy. *J. Controlled Release* **2019**, *301*, 157.

(79) Song, J.; Lin, L.; Yang, Z.; Zhu, R.; Zhou, Z.; Li, Z.; Wang, F.; Chen, J.; Yang, H.; Chen, X. Self-assembled responsive bilayered vesicles with adjustable oxidative stress for enhanced cancer imaging and therapy. *J. Am. Chem. Soc.* **2019**, *141*, 8158.

(80) Duan, B.; Wang, D.; Wu, H.; Xu, P.; Jiang, P.; Xia, G.; Liu, Z.; Wang, H.; Guo, Z.; Chen, Q. Core-shell structured Fe(3)O(4)@C@MnO(2) nanoparticles as pH responsive T(1)-T(2)* dual-modal contrast agents for tumor diagnosis. *ACS Biomater. Sci. Eng.* **2018**, *4*, 3047.

(81) Lu, H.; Chen, A.; Zhang, X.; Wei, Z.; Cao, R.; Zhu, Y.; Lu, J.; Wang, Z.; Tian, L. A pH-responsive T(1)-T(2) dual-modal MRI contrast agent for cancer imaging. *Nat. Commun.* **2022**, *13*, 7948.

(82) Lin, C. W.; Tseng, S. J.; Kempson, I. M.; Yang, S. C.; Hong, T. M.; Yang, P. C. Extracellular delivery of modified oligonucleotide and superparamagnetic iron oxide nanoparticles from a degradable hydrogel triggered by tumor acidosis. *Biomaterials* **2013**, *34*, 4387.

(83) Gao, G. H.; Im, G. H.; Kim, M. S.; Lee, J. W.; Yang, J.; Jeon, H.; Lee, J. H.; Lee, D. S. Magnetite-nanoparticle-encapsulated pH-responsive polymeric micelle as an MRI probe for detecting acidic pathologic areas. *Small* **2010**, *6*, 1201.

(84) Choi, J. S.; Kim, S.; Yoo, D.; Shin, T. H.; Kim, H.; Gomes, M. D.; Kim, S. H.; Pines, A.; Cheon, J. Distance-dependent magnetic resonance tuning as a versatile MRI sensing platform for biological targets. *Nat. Mater.* **2017**, *16*, 537.

(85) Phung, C. D.; Tran, T. H.; Pham, L. M.; Nguyen, H. T.; Jeong, J. H.; Yong, C. S.; Kim, J. O. Current developments in nanotechnology for improved cancer treatment, focusing on tumor hypoxia. *J. Controlled Release* **2020**, *324*, 413.

(86) Zhou, H.; Qin, F.; Chen, C. Designing hypoxia-responsive nanotheranostic agents for tumor imaging and therapy. *Adv. Healthc Mater.* **2021**, *10*, e2001277.

(87) Filippi, M.; Nguyen, D. V.; Garello, F.; Perton, F.; Begin-Colin, S.; Felder-Flesch, D.; Power, L.; Scherberich, A. Metronidazole-functionalized iron oxide nanoparticles for molecular detection of hypoxic tissues. *Nanoscale* **2019**, *11*, 22559.

(88) Zhou, H.; Guo, M.; Li, J.; Qin, F.; Wang, Y.; Liu, T.; Liu, J.; Sabet, Z. F.; Wang, Y.; Liu, Y.; Huo, Q.; Chen, C. Hypoxia-triggered self-assembly of ultrasmall iron oxide nanoparticles to amplify the imaging signal of a tumor. *J. Am. Chem. Soc.* **2021**, *143*, 1846.

(89) Yang, L.; Afshari, M. J.; Ge, J.; Kou, D.; Chen, L.; Zhou, D.; Li, C.; Wu, S.; Zhang, L.; Zeng, J.; Zhong, J.; Stauber, R. H.; Gao, M. Functionalized ultrasmall iron oxide nanoparticles for T1-weighted magnetic resonance imaging of tumor hypoxia. *Molecules* **2022**, *27*, 6929.

(90) Martínez-Reyes, I.; Chandel, N. S. Cancer metabolism: looking forward. *Nat. Rev. Cancer* **2021**, *21*, 669.

(91) R, S.; M Joseph, M.; Sen, A.; K, R. P.; BS, U.; TT, S. Galactomannan armed superparamagnetic iron oxide nanoparticles as a folate receptor targeted multi-functional theranostic agent in the management of cancer. *Int. J. Biol. Macromol.* **2022**, *219*, 740.

(92) Yin, S.; Huai, J.; Chen, X.; Yang, Y.; Zhang, X.; Gan, Y.; Wang, G.; Gu, X.; Li, J. Intracellular delivery and antitumor effects of a redox-responsive polymeric paclitaxel conjugate based on hyaluronic acid. *Acta Biomater* **2015**, *26*, 274.

(93) Cao, Y.; Mao, Z.; He, Y.; Kuang, Y.; Liu, M.; Zhou, Y.; Zhang, Y.; Pei, R. Extremely small iron oxide nanoparticle-encapsulated nanogels as a glutathione-responsive T1 contrast agent for tumor-targeted magnetic resonance imaging. *ACS Appl. Mater. Interfaces* **2020**, *12*, 26973.

(94) Ma, D.; Shi, M.; Li, X.; Zhang, J.; Fan, Y.; Sun, K.; Jiang, T.; Peng, C.; Shi, X. Redox-sensitive clustered ultrasmall iron oxide nanoparticles for switchable T2/T1-weighted magnetic resonance imaging applications. *Bioconjug Chem.* **2020**, *31*, 352.

(95) Liu, D.; Zhou, Z.; Wang, X.; Deng, H.; Sun, L.; Lin, H.; Kang, F.; Zhang, Y.; Wang, Z.; Yang, W.; Rao, L.; Yang, K.; Yu, G.; Du, J.; Shen, Z.; Chen, X. Yolk-shell nanovesicles endow glutathione-responsive concurrent drug release and T1MRI activation for cancer theranostics. *Biomaterials* **2020**, *244*, 119979.

(96) Liu, Y.; Yang, Z.; Huang, X.; Yu, G.; Wang, S.; Zhou, Z.; Shen, Z.; Fan, W.; Liu, Y.; Davisson, M.; Kalish, H.; Niu, G.; Nie, Z.; Chen, X. Glutathione-responsive self-assembled magnetic Gold nanowreath for enhanced tumor imaging and imaging-guided photothermal therapy. *ACS Nano* **2018**, *12*, 8129.

(97) Wang, C.; Yan, C.; An, L.; Zhao, H.; Song, S.; Yang, S. Fe3O4 assembly for tumor accurate diagnosis by endogenous GSH responsive T2/T1 magnetic relaxation conversion. *J. Mater. Chem. B* **2021**, *9*, 7734.

(98) Li, T.; Rao, B.; Xu, D.; Zhou, J.; Sun, W.; Zhi, X.; Zhang, C.; Cui, D.; Xu, H. Enzyme-like copper-encapsulating magnetic nano-assemblies for switchable T1-weighted MRI and potentiating chemo-/photo-dynamic therapy. *Acta Biomater* **2022**, *153*, 431.

(99) Xu, X.; Zhou, X.; Xiao, B.; Xu, H.; Hu, D.; Qian, Y.; Hu, H.; Zhou, Z.; Liu, X.; Gao, J.; Slater, N.; Shen, Y.; Tang, J. Glutathione-responsive magnetic nanoparticles for highly sensitive diagnosis of liver metastases. *Nano Lett.* **2021**, *21*, 2199.

(100) Wu, B.; Deng, K.; Lu, S. T.; Zhang, C. J.; Ao, Y. W.; Wang, H.; Mei, H.; Wang, C. X.; Xu, H.; Hu, B.; Huang, S. W. Reduction-active Fe(3)O(4)-loaded micelles with aggregation- enhanced MRI contrast for differential diagnosis of Neroglioma. *Biomaterials* **2021**, *268*, 120531.

(101) Gao, Z.; Hou, Y.; Zeng, J.; Chen, L.; Liu, C.; Yang, W.; Gao, M. Tumor microenvironment-triggered aggregation of anti-phagocytosis 99mTc-labelled Fe3O4 nanoprobes for enhanced tumor imaging in vivo. *Adv. Mater.* **2017**, *29*, 1701095.

(102) Zhang, P.; Zeng, J.; Li, Y.; Yang, C.; Meng, J.; Hou, Y.; Gao, M. Quantitative mapping of glutathione within intracranial tumors through interlocked MRI signals of a responsive nanoprobe. *Angew. Chem., Int. Ed. Engl.* **2021**, *60*, 8130.

(103) Kim, M. H.; Son, H. Y.; Kim, G. Y.; Park, K.; Huh, Y. M.; Haam, S. Redoxable heteronanocrystals functioning magnetic relaxation switch for activatable T1 and T2 dual-mode magnetic resonance imaging. *Biomaterials* **2016**, *101*, 121.

(104) Li, J.; Wang, S.; Wu, C.; Dai, Y.; Hou, P.; Han, C.; Xu, K. Activatable molecular MRI nanoprobe for tumor cell imaging based

on gadolinium oxide and iron oxide nanoparticle. *Biosens Bioelectron* **2016**, *86*, 1047.

(105) Wang, Z.; Xue, X.; Lu, H.; He, Y.; Lu, Z.; Chen, Z.; Yuan, Y.; Tang, N.; Dreyer, C. A.; Quigley, L.; Curro, N.; Lam, K. S.; Walton, J. H.; Lin, T. Y.; Louie, A. Y.; Gilbert, D. A.; Liu, K.; Ferrara, K. W.; Li, Y. Two-way magnetic resonance tuning and enhanced subtraction imaging for non-invasive and quantitative biological imaging. *Nat. Nanotechnol* **2020**, *15*, 482.

(106) Ding, J.; Guan, Y.; Cong, Y.; Chen, L.; Li, Y. F.; Zhang, L.; Zhang, L.; Wang, J.; Bai, R.; Zhao, Y.; Chen, C.; Wang, L. Single-particle analysis for structure and iron chemistry of atmospheric particulate matter. *Anal. Chem.* **2020**, *92*, 975.

(107) Renzulli, M.; Clemente, A.; Ierardi, A. M.; Pettinari, I.; Tovoli, F.; Brocchi, S.; Peta, G.; Cappabianca, S.; Carrafiello, G.; Golfieri, R. Imaging of colorectal liver metastases: new developments and pending issues. *Cancers* **2020**, *12*, 151.

(108) Santra, S.; Jativa, S. D.; Kaittanis, C.; Normand, G.; Grimm, J.; Perez, J. M. Gadolinium-encapsulating iron oxide nanoprobe as activatable NMR/MRI contrast agent. *ACS Nano* **2012**, *6*, 7281.

(109) Guo, H.; Song, S.; Dai, T.; Sun, K.; Zhou, G.; Li, M.; Mann, S.; Dou, H. Near-infrared fluorescent and magnetic resonance dual-imaging coacervate nanoprobes for trypsin mapping and targeted payload delivery of malignant tumors. *ACS Appl. Mater. Interfaces* **2020**, *12*, 17302.

(110) Gallo, J.; Kamaly, N.; Lavdas, I.; Stevens, E.; Nguyen, Q. D.; Wylezinska-Arridge, M.; Aboagye, E. O.; Long, N. J. CXCR4-targeted and MMP-responsive iron oxide nanoparticles for enhanced magnetic resonance imaging. *Angew. Chem., Int. Ed. Engl.* **2014**, *53*, 9550.

(111) Yuan, Y.; Ding, Z.; Qian, J.; Zhang, J.; Xu, J.; Dong, X.; Han, T.; Ge, S.; Luo, Y.; Wang, Y.; Zhong, K.; Liang, G. Casp3/7-instructed intracellular aggregation of Fe3O4 nanoparticles enhances T2MR imaging of tumor apoptosis. *Nano Lett.* **2016**, *16*, 2686.

(112) Wang, Y.; Li, X.; Chen, P.; Dong, Y.; Liang, G.; Yu, Y. Enzyme-instructed self-aggregation of Fe(3)O(4) nanoparticles for enhanced MRI T(2) imaging and photothermal therapy of tumors. *Nanoscale* **2020**, *12*, 1886.

(113) Choi, J. S.; Lee, J. H.; Shin, T. H.; Song, H. T.; Kim, E. Y.; Cheon, J. Self-confirming "AND" logic nanoparticles for fault-free MRI. *J. Am. Chem. Soc.* **2010**, *132*, 11015.

(114) Zhu, X.; Lin, H.; Wang, L.; Tang, X.; Ma, L.; Chen, Z.; Gao, J. Activatable T1 relaxivity recovery nanoconjugates for kinetic and sensitive analysis of matrix metalloprotease 2. *ACS Appl. Mater. Interfaces* **2017**, *9*, 21688.

(115) Manchanda, M.; Das, P.; Gahlot, G. P S; Singh, R.; Roeb, E.; Roderfeld, M.; Gupta, S. D.; Saraya, A.; Pandey, R M; Chauhan, S. S Cathepsin L and B as potential markers for liver fibrosis: insights from patients and experimental models. *Clin Transl Gastroenterol* **2017**, *8*, e99.

(116) Banstola, A.; Poudel, K.; Kim, J. O.; Jeong, J. H.; Yook, S. Recent progress in stimuli-responsive nanosystems for inducing immunogenic cell death. *J. Controlled Release* **2021**, *337*, 505.

(117) Jing, X.; Xu, Y.; Liu, D.; Wu, Y.; Zhou, N.; Wang, D.; Yan, K.; Meng, L. Intelligent nanoflowers: a full tumor microenvironment-responsive multimodal cancer theranostic nanoplatform. *Nanoscale* **2019**, *11*, 15508.

(118) Ren, S.; Yang, J.; Ma, L.; Li, X.; Wu, W.; Liu, C.; He, J.; Miao, L. Ternary-responsive drug delivery with activatable dual mode contrast-enhanced in vivo imaging. *ACS Appl. Mater. Interfaces* **2018**, *10*, 31947.

(119) Liu, W.; Yin, S.; Hu, Y.; Deng, T.; Li, J. Microemulsion-confined assembly of magnetic nanoclusters for pH/H2O2 dual-responsive T2-T1 switchable MRI. *ACS Appl. Mater. Interfaces* **2022**, *14*, 2629.

(120) Song, X. R.; Li, S. H.; Dai, J.; Song, L.; Huang, G.; Lin, R.; Li, J.; Liu, G.; Yang, H. H. Polyphenol-inspired facile construction of smart assemblies for ATP- and pH-responsive tumor MR/optical imaging and photothermal therapy. *Small* **2017**, *13*, 1603997.

(121) Zhou, H.; Tang, J.; Li, J.; Li, W.; Liu, Y.; Chen, C. In vivo aggregation-induced transition between T1 and T2 relaxations of magnetic ultra-small iron oxide nanoparticles in tumor microenvironment. *Nanoscale* **2017**, *9*, 3040.

(122) Lin, J.; Xin, P.; An, L.; Xu, Y.; Tao, C.; Tian, Q.; Zhou, Z.; Hu, B.; Yang, S. Fe(3)O(4)-ZIF-8 assemblies as pH and glutathione responsive T(2)-T(1) switching magnetic resonance imaging contrast agent for sensitive tumor imaging in vivo. *Chem. Commun.* **2019**, *55*, 478.

(123) Sun, X.; Zhang, G.; Du, R.; Xu, R.; Zhu, D.; Qian, J.; Bai, G.; Yang, C.; Zhang, Z.; Zhang, X.; Zou, D.; Wu, Z. A biodegradable MnSiO3@Fe3O4 nanoplatform for dual-mode magnetic resonance imaging guided combinatorial cancer therapy. *Biomaterials* **2019**, *194*, 151.

(124) Wan, L.; Chen, Z.; Deng, Y.; Liao, T.; Kuang, Y.; Liu, J.; Duan, J.; Xu, Z.; Jiang, B.; Li, C. A novel intratumoral pH/redox-dual-responsive nanoplatform for cancer MR imaging and therapy. *J. Colloid Interface Sci.* **2020**, *573*, 263.

(125) Peng, N.; Ding, X.; Wang, Z.; Cheng, Y.; Gong, Z.; Xu, X.; Gao, X.; Cai, Q.; Huang, S.; Liu, Y. Novel dual responsive alginate-based magnetic nanogels for onco-theranostics. *Carbohydr. Polym.* **2019**, *204*, 32.

(126) Xu, R.; Xu, Z.; Si, Y.; Xing, X.; Li, Q.; Xiao, J.; Wang, B.; Tian, G.; Zhu, L.; Wu, Z.; Zhang, G. Oxygen vacancy defect-induced activity enhancement of Gd doping magnetic nanocluster for oxygen supplying cancer theranostics. *ACS Appl. Mater. Interfaces* **2020**, *12*, 36917.

(127) Mohamed M, S.; Veeranarayanan, S.; Maekawa, T.; Kumar D, S. External stimulus responsive inorganic nanomaterials for cancer theranostics. *Adv. Drug Deliv Rev.* **2019**, *138*, 18.

(128) Zhang, F.; Lu, G.; Wen, X.; Li, F.; Ji, X.; Li, Q.; Wu, M.; Cheng, Q.; Yu, Y.; Tang, J.; Mei, L. Magnetic nanoparticles coated with polyphenols for spatio-temporally controlled cancer photo-thermal/immunotherapy. *J. Controlled Release* **2020**, *326*, 131.

(129) Guo, Y.; Ran, Y.; Wang, Z.; Cheng, J.; Cao, Y.; Yang, C.; Liu, F.; Ran, H. Magnetic-responsive and targeted cancer nanotheranostics by PA/MR bimodal imaging-guided photothermally triggered immunotherapy. *Biomaterials* **2019**, *219*, 119370.

(130) Kilinc, D.; Dennis, C. L.; Lee, G. U. Bio-nano-magnetic materials for localized mechanochemical stimulation of cell growth and death. *Adv. Mater.* **2016**, *28*, 5672.

(131) Bai, J.; Wang, J. T.; Rubio, N.; Protti, A.; Heidari, H.; Elgogary, R.; Southern, P.; Al-Jamal, W. T.; Sosabowski, J.; Shah, A. M.; Bals, S.; Pankhurst, Q. A.; Al-Jamal, K. T. Triple-modal imaging of magnetically-targeted nanocapsules in solid tumours in vivo. *Theranostics* **2016**, *6*, 342.

(132) Yang, T.; Niu, D.; Chen, J.; He, J.; Yang, S.; Jia, X.; Hao, J.; Zhao, W.; Li, Y. Biodegradable organosilica magnetic micelles for magnetically targeted MRI and GSH-triggered tumor chemotherapy. *Biomater Sci.* **2019**, *7*, 2951.

(133) Li, E.; Yang, Y.; Hao, G.; Yi, X.; Zhang, S.; Pan, Y.; Xing, B.; Gao, M. Multifunctional magnetic mesoporous silica nanoagents forin vivo enzyme-responsive drug delivery and MR imaging. *Nano-theranostics* **2018**, *2*, 233.

(134) Liu, Y.; Li, J.; Chen, H.; Cai, Y.; Sheng, T.; Wang, P.; Li, Z.; Yang, F.; Gu, N. Magnet-activatable nanoliposomes as intracellular bubble microreactors to enhance drug delivery efficacy and burst cancer cells. *Nanoscale* **2019**, *11*, 18854.

(135) Yang, K.; Liu, Y.; Liu, Y.; Zhang, Q.; Kong, C.; Yi, C.; Zhou, Z.; Wang, Z.; Zhang, G.; Zhang, Y.; Khashab, N. M.; Chen, X.; Nie, Z. Cooperative assembly of magneto-nanovesicles with tunable wall thickness and permeability for MRI-guided drug delivery. *J. Am. Chem. Soc.* **2018**, *140*, 4666.

(136) Chen, L.; Wu, Y.; Wu, H.; Li, J.; Xie, J.; Zang, F.; Ma, M.; Gu, N.; Zhang, Y. Magnetic targeting combined with active targeting of dual-ligand iron oxide nanoprobes to promote the penetration depth in tumors for effective magnetic resonance imaging and hyperthermia. *Acta Biomater* **2019**, *96*, 491.

(137) Licciardi, M.; Scialabba, C.; Puleio, R.; Cassata, G.; Cicero, L.; Cavallaro, G.; Giammona, G. Smart copolymer coated SPIONs for colon cancer chemotherapy. *Int. J. Pharm.* **2019**, *556*, 57.

(138) Chen, H.; Zhao, Y. Applications of light-responsive systems for cancer theranostics. *ACS Appl. Mater. Interfaces* **2018**, *10*, 21021.

(139) Osborne, E. A.; Jarrett, B. R.; Tu, C.; Louie, A. Y. Modulation of T2 relaxation time by light-induced, reversible aggregation of magnetic nanoparticles. *J. Am. Chem. Soc.* **2010**, *132*, 5934.

(140) Deng, K.; Wu, B.; Wang, C. X.; Wang, Q.; Yu, H.; Li, J. M.; Li, K. H.; Zhao, H. Y.; Huang, S. W. An oxidation-enhanced magnetic resonance imaging probe for visual and specific detection of singlet oxygen generated in photodynamic cancer therapy in vivo. *Adv. Healthc Mater.* **2020**, *9*, e2000533.

(141) Li, X.; Lu, S.; Xiong, Z.; Hu, Y.; Ma, D.; Lou, W.; Peng, C.; Shen, M.; Shi, X. Light-addressable nanoclusters of ultrasmall iron oxide nanoparticles for enhanced and dynamic magnetic resonance imaging of arthritis. *Adv. Sci.* **2019**, *6*, 1901800.

(142) Hannecart, A.; Stanicki, D.; Vander Elst, L.; Muller, R. N.; Lecommandoux, S.; Thévenot, J.; Bonduelle, C.; Trotier, A.; Massot, P.; Miraux, S.; Sandre, O.; Laurent, S. Nano-thermometers with thermo-sensitive polymer grafted USPIOs behaving as positive contrast agents in low-field MRI. *Nanoscale* **2015**, *7*, 3754.

(143) Chung, I. J.; Moon, H.; Jeon, S. I.; Lee, H. J.; Ahn, C. H. Ultrasound-triggered imaging and drug delivery using microbubble-self-aggregate complexes. *J. Biomater Sci. Polym. Ed* **2022**, *33*, 57.

(144) Yang, F.; Zhang, M.; He, W.; Chen, P.; Cai, X.; Yang, L.; Gu, N.; Wu, J. Controlled release of Fe3O4 nanoparticles in encapsulated microbubbles to tumor cells via sonoporation and associated cellular bioeffects. *Small* **2011**, *7*, 902.

(145) Lee, S. F.; Zhu, X. M.; Wang, Y. X.; Xuan, S. H.; You, Q.; Chan, W. H.; Wong, C. H.; Wang, F.; Yu, J. C.; Cheng, C. H.; Leung, K. C. Ultrasound, pH, and magnetically responsive crown-ether-coated core/shell nanoparticles as drug encapsulation and release systems. *ACS Appl. Mater. Interfaces* **2013**, *5*, 1566.

(146) Gou, M.; Li, S.; Zhang, L.; Li, L.; Wang, C.; Su, Z. Facile one-pot synthesis of carbon/calcium phosphate/Fe3O4 composite nanoparticles for simultaneous imaging and pH/NIR-responsive drug delivery. *Chem. Commun.* **2016**, *52*, 11068.

(147) Khafaji, M.; Zamani, M.; Vossoughi, M.; Iraji zad, A. Doxorubicin/cisplatin-loaded superparamagnetic nanoparticles as a stimuli-responsive co-delivery system for chemo-photothermal therapy. *Int. J. Nanomedicine* **2019**, *14*, 8769.

(148) Zhang, M.; Wang, W.; Wu, F.; Graveran, K.; Zhang, J.; Wu, C. Black phosphorus quantum dots gated, carbon-coated Fe(3)O(4) nanocapsules (BPQDs@ss-Fe(3)O(4)@C) with low premature release could enable imaging-guided cancer combination therapy. *Chemistry* **2018**, *24*, 12890.

(149) Zhang, Y.; Li, F.; Ya, S.; Hu, Y.; Zhi, D.; Wang, W.; Xu, M.; Qiu, B.; Ding, W. An iron oxide nanoparticle-based transdermal nanoplatform for dual-modal imaging-guided chemo-photothermal therapy of superficial tumors. *Acta Biomater* **2021**, *130*, 473.

(150) Liu, N.; Wu, L.; Zuo, W.; Lin, Q.; Liu, J.; Jin, Q.; Xiao, Z.; Chen, L.; Zhao, Y.; Zhou, J.; Zhu, X. pH/Thermal-sensitive nanoplatform capable of on-demand specific release to potentiate drug delivery and combinational hyperthermia/chemo/chemodynamic therapy. *ACS Appl. Mater. Interfaces* **2022**, *14*, 29668.

(151) Wu, F.; Zhang, M.; Lu, H.; Liang, D.; Huang, Y.; Xia, Y.; Hu, Y.; Hu, S.; Wang, J.; Yi, X.; Zhang, J. Triple stimuli-responsive magnetic hollow porous carbon-based nanodrug delivery system for magnetic resonance imaging-guided synergistic photothermal/chemo-therapy of cancer. *ACS Appl. Mater. Interfaces* **2018**, *10*, 21939.

(152) Chen, C.; Ge, J.; Gao, Y.; Chen, L.; Cui, J.; Zeng, J.; Gao, M. Ultrasmall superparamagnetic iron oxide nanoparticles: a next generation contrast agent for magnetic resonance imaging. *Wiley Interdiscip Rev. Nanomed Nanobiotechnol* **2022**, *14*, e1740.

(153) Zhou, H.; Hou, X.; Liu, Y.; Zhao, T.; Shang, Q.; Tang, J.; Liu, J.; Wang, Y.; Wu, Q.; Luo, Z.; Wang, H.; Chen, C. Superstable magnetic nanoparticles in conjugation with near-infrared dye as a multimodal theranostic platform. *ACS Appl. Mater. Interfaces* **2016**, *8*, 4424.

(154) Hou, X.; Zhou, H.; Wang, L.; Tang, J.; Chen, C.; Jiang, G.; Liu, Y. Multifunctional near-infrared dye-magnetic nanoparticles for bioimaging and cancer therapy. *Cancer Lett.* **2017**, *390*, 168.

(155) Cai, Y.; Hofstetter, S.; van der Zwaag, W.; Zuiderbaan, W.; Dumoulin, S. O. Individualized cognitive neuroscience needs 7T: comparing numerosity maps at 3T and 7T MRI. *Neuroimage* **2021**, *237*, 118184.

(156) Liu, T.; Bai, R.; Zhou, H.; Wang, R.; Liu, J.; Zhao, Y.; Chen, C. The effect of size and surface ligands of iron oxide nanoparticles on blood compatibility. *RSC Adv.* **2020**, *10*, 7559.

(157) Vakili-Ghartavol, R.; Momtazi-Borojeni, A. A.; Vakili-Ghartavol, Z.; Aiyelabegan, H. T.; Jaafari, M. R.; Rezayat, S. M.; Arbabi Bidgoli, S. Toxicity assessment of superparamagnetic iron oxide nanoparticles in different tissues. *Artif Cells Nanomed Biotechnol* **2020**, *48*, 443.

(158) Li, J.; Chen, C.; Xia, T. Understanding nanomaterial-liver interactions to facilitate the development of safer nanoapplications. *Adv. Mater.* **2022**, *34*, 2106456.

(159) Ren, J.; Andrikopoulos, N.; Velonia, K.; Tang, H.; Cai, R.; Ding, F.; Ke, P. C.; Chen, C. Chemical and biophysical signatures of the protein corona in nanomedicine. *J. Am. Chem. Soc.* **2022**, *144*, 9184.

(160) Cai, R.; Chen, C. The crown and the scepter: roles of the protein corona in nanomedicine. *Adv. Mater.* **2019**, *31*, e1805740.

(161) Rabel, M.; Warncke, P.; Thürmer, M.; Grüttner, C.; Bergemann, C.; Kurland, H. D.; Müller, F. A.; Koeberle, A.; Fischer, D. The differences of the impact of a lipid and protein corona on the colloidal stability, toxicity, and degradation behavior of iron oxide nanoparticles. *Nanoscale* **2021**, *13*, 9415.

(162) Wang, X.; Lei, R.; Li, L.; Fei, X.; Ju, R.; Sun, X.; Cao, H.; Zhang, Q.; Chen, C.; Wang, X. Rearrangement of protein structures on a gold nanoparticle surface is regulated by ligand adsorption modes. *Nanoscale* **2021**, *13*, 20425.

(163) Ren, J.; Cai, R.; Wang, J.; Daniyal, M.; Baimanov, D.; Liu, Y.; Yin, D.; Liu, Y.; Miao, Q.; Zhao, Y.; Chen, C. Precision nanomedicine development based on specific opsonization of human cancer patient-personalized protein coronas. *Nano Lett.* **2019**, *19*, 4692.

(164) Zhang, G.; Cong, Y.; Liu, F. L.; Sun, J.; Zhang, J.; Cao, G.; Zhou, L.; Yang, W.; Song, Q.; Wang, F.; Liu, K.; Qu, J.; Wang, J.; He, M.; Feng, S.; Baimanov, D.; Xu, W.; Luo, R. H.; Long, X. Y.; Liao, S.; Fan, Y.; Li, Y. F.; Li, B.; Shao, X.; Wang, G.; Fang, L.; Wang, H.; Yu, X. F.; Chang, Y. Z.; Zhao, Y.; Li, L.; Yu, P.; Zheng, Y. T.; Boraschi, D.; Li, H.; Chen, C.; Wang, L.; Li, Y. A nanomaterial targeting the spike protein captures SARS-CoV-2 variants and promotes viral elimination. *Nat. Nanotechnol* **2022**, *17*, 993.

(165) Baimanov, D.; Wang, J.; Zhang, J.; Liu, K.; Cong, Y.; Shi, X.; Zhang, X.; Li, Y.; Li, X.; Qiao, R.; Zhao, Y.; Zhou, Y.; Wang, L.; Chen, C. In situ analysis of nanoparticle soft corona and dynamic evolution. *Nat. Commun.* **2022**, *13*, 5389.

(166) Wang, L.; Quan, P.; Chen, S. H.; Bu, W.; Li, Y. F.; Wu, X.; Wu, J.; Zhang, L.; Zhao, Y.; Jiang, X.; Lin, B.; Zhou, R.; Chen, C. Stability of ligands on nanoparticles regulating the integrity of biological membranes at the nano-lipid interface. *ACS Nano* **2019**, *13*, 8680.

(167) Ding, J.; Guan, Y.; Cong, Y.; Chen, L.; Li, Y. F.; Zhang, L.; Zhang, L.; Wang, J.; Bai, R.; Zhao, Y.; Chen, C.; Wang, L. Single-particle analysis for structure and iron chemistry of atmospheric particulate matter. *Anal. Chem.* **2020**, *92*, 975.

(168) Wang, L.; Zhang, T.; Li, P.; Huang, W.; Tang, J.; Wang, P.; Liu, J.; Yuan, Q.; Bai, R.; Li, B.; Zhang, K.; Zhao, Y.; Chen, C. Use of synchrotron radiation-analytical techniques to reveal chemical origin of silver-nanoparticle cytotoxicity. *ACS Nano* **2015**, *9*, 6532.

(169) Li, J.; Zhang, Q.; Che, Y.; Zhang, N.; Guo, L. Iron deposition characteristics of deep gray matter in elderly individuals in the community revealed by quantitative susceptibility mapping and multiple factor analysis. *Front Aging Neurosci* **2021**, *13*, 611891.

(170) Bring, P.; Partovi, N.; Ford, J. A.; Yoshida, E. M. Iron overload disorders: treatment options for patients refractory to or intolerant of phlebotomy. *Pharmacotherapy* **2008**, *28*, 331.

(171) Liu, Q.; Zhao, Y.; Zhou, H.; Chen, C. Ferroptosis: challenges and opportunities for nanomaterials in cancer therapy. *Regen Biomater* **2023**, *10*, rbad004.

(172) Bi, W. L.; Hosny, A.; Schabath, M. B.; Giger, M. L.; Birkbak, N. J.; Mehrtash, A.; Allison, T.; Arnaout, O.; Abbosh, C.; Dunn, I. F.; Mak, R. H.; Tamimi, R. M.; Tempany, C. M.; Swanton, C.; Hoffmann, U.; Schwartz, L. H.; Gillies, R. J.; Huang, R. Y.; Aerts, H. J. W. L. Artificial intelligence in cancer imaging: Clinical challenges and applications. *CA Cancer J. Clin.* **2019**, *69*, 127.

(173) Bera, K.; Braman, N.; Gupta, A.; Velcheti, V.; Madabhushi, A. Predicting cancer outcomes with radiomics and artificial intelligence in radiology. *Nat. Rev. Clin Oncol* **2022**, *19*, 132.

(174) Gillies, R. J.; Kinahan, P. E.; Hricak, H. Radiomics: images are more than pictures, they are data. *Radiology* **2016**, *278*, 563.